Direction of Arrival Estimation Technique for Narrow-Band Signals Based on Spatial Discrete Fourier Transform

by

Ramin Zaeim
M.Sc., Science and Research Azad University, Tehran, Iran, 2010
B.Sc., Science and Research Azad University, Tehran, Iran, 2006

A Thesis Submitted in Partial Fulfillment
of the Requirements for the Degree of

MASTER OF APPLIED SCIENCE

in the Department of Electrical and Computer Engineering

Direction of Arrival Estimation Technique for Narrow-Band signals Based on Spatial Discrete Fourier Transform

by

Ramin Zaeim
M.Sc., Science and Research Azad University, Tehran, Iran, 2010
B.Sc., Science and Research Azad University, Tehran, Iran, 2006

Supervisory Committee

Dr. Panjotis Agathoklis, Supervisor
(Department of Electrical & Computer Engineering)

Dr. Dale Shpak, Departmental member
(Department of Electrical & Computer Engineering)

Dr. Yang Shi, Outside member
(Department of Mechanical Engineering)

Supervisory Committee

Dr. Panjotis Agathoklis, Supervisor
(Department of Electrical & Computer Engineering)

Dr. Dale Shpak, Departmental member
(Department of Electrical & Computer Engineering)

Dr. Yang Shi, Outside member
(Department of Mechanical Engineering)

Abstract

This work deals with the further development of a method for Direction of Arrival (DOA) estimation based on the Discrete Fourier Transform (DFT) of the sensor array output. In the existing DFT-based algorithm, relatively high SNR is considered, and it is assumed that a large number of sensors are available.

In this study an overview of some of the most commonly used DOA estimation techniques will be presented. Then the performance of the DFT method will be analyzed and compared with the performance of existing techniques. Two main objectives will be studied, firstly the reduction of the number of sensors and secondly the performance of the DFT based technique in the presence of noise.

Experimental simulations will be presented to illustrate that in absence of noise, the proposed method is very fast and using just one snapshot is sufficient to accurately estimate DOAs. Also, in

presence of noise, the method is still relatively fast and using a small number of snapshots, it can accurately estimate DOAs.

The above mentioned properties are the result of taking an average of the peaks of the DFTs, $\boldsymbol{X}_n(k)$, obtained from a sequence of N_s snapshots. With N_s sufficiently large, the average over N_s snapshots approaches expected value. Also, the conditions that should be satisfied to avoid overlapping of main-lobes, and thus loosing the DOA of some signals, in the DFT spectrum are examined.

This study further analyzes the performance of the proposed method as well as two other commonly used algorithms, MUSIC and conventional beamformer. An extensive simulation was conducted and different features of the spatial DFT technique, such as accuracy, resolution, sensitivity to noise, effect of multiple snapshots and the number of sensors were evaluated and compared with those of existing techniques. The simulations indicate that in most aspects the proposed spatial DFT algorithm outperforms the other techniques.

Table of Contents

List of Figures

List of Abbreviation

BER	Bit Error Rate
DCT	Discrete Cosine Transform
DOA	Direction Of Arrival
DCT	Discrete Fourier Transform
DFT	Discrete Fourier Transform
ESPRIT	Estimation of Signal Parameters via Rotational Invariance Technique
FFT	Fast Fourier Transform
MUSIC	Multiple Signal Classification
MVDR.	Minimum Variance Distortion-less Response
ML	Maximum Likelihood
RMSD	Root Mean Square Deviation
SNR	Signal to Noise Ratio
SVD	Singular Value Decomposition
TLS	Total Least Squares
ULA	Uniform Linear Array

Notation

Unless stated otherwise, lower case letters indicate scalers and boldface upper-case and lower-case letters denote matrices and vectors respectively. Also, italic boldface upper-case represent frequency domain.

A^{-1}	the inverse of matrix A
A^T	the transpose of matrix A
A^H	the Hermitian transpose of matrix A
$E[\boldsymbol{a}\boldsymbol{a}^H]$	correlation matrix of $\boldsymbol{a}$
$E[x]$	Expected value of x
$A \perp B$	Vectors of A are orthogonal to vectors in B
$\boldsymbol{X}^n(k)$	K point DFT of received signal at the antenna at the n^{th} sample
$\hat{A}$	Estimation of A
$\|A\|$	Absolute value of A
Re $\{A\}$	Real part of A
Im $\{A\}$	Imaginary part of A
$\angle a$	Phase of a

Acknowledgments

First and foremost, I would like to express my sincere appreciation to my supervisor Professor Pan Agathoklis for all his invaluable support, encouragement and guidance. His precise and regular supervision, invaluable and critical suggestions, and friendly treatment made the way through my master's study. His office door has always been open for me and he has always treated me like a friend. He had a remarkable ability to break down a complicated problem into simpler steps which follow a logical line so that I could understand not only how to deal with the problem, but why it was solved that way.

I would also like to thank my supervisory committee member Professor Dale Shpak for offering me valuable comments and suggestions.

I am very grateful to UVic staff, specially Mr. Dan Mai, Ms. Amy Issel, Ms. Ashleigh Burns, Mr. Kevin Jones, Mr. Rob Fichtner and Professor Wu-Sheng Lu.

I would like to express my deepest gratitude to my parents and my sister who have always supported me through my whole life and have never deprived me of a chance to be a better person. At the end, I would like to extend my endless thanks and appreciation to my lovely wife Arezoo, for her unconditional support, help, love and patience.

Dedication

Dedicated to my beloved parents and wife

For their unconditional support and endless love

Chapter 1

Introduction

1.1 Introduction

The need for Array Signal Processing arises in many engineering applications including wireless communications, radar, radio astronomy, sonar, navigation, tracking of various objects, rescue and other emergency assistance devices. Much of the work in this field, especially in earlier days, focused on radio direction finding, that is estimating the direction of electromagnetic waves impinging on one or more antennas [1].

The capacity of wireless communication systems can be increased by adding additional carrier frequencies. Following the increasing over usage of the low end of the spectrum, people started to explore the higher frequency bands for these applications, where more spectrum is available. With higher frequencies, higher data rate and higher user density, multipath fading and cross interference become more serious issues, resulting in the degradation of bit error rate (BER). One possibility to combat these problems and to achieve higher communication capacity is to use smart antenna systems with adaptive beamforming capability. They have proven to be very effective in suppression of the interference and multipath signals [2]. Instead of using a single antenna, array antenna systems, which have multiple sensors distributed in space, offer increased gain (range), reduced interference, more power efficiency and provide spatial diversity [3]. By being able to determine and track the directions of users in the coverage area and directionally transmit and

receive, smart antennas have enhanced the ability of the communication systems in terms of coverage, quality of service, and throughput [4].

One important problem of smart antenna systems is the development of efficient algorithms for Direction-of-Arrival (DOA) estimation and adaptive beamforming. Recent trends in these areas drive the development of digital beamforming systems [5].

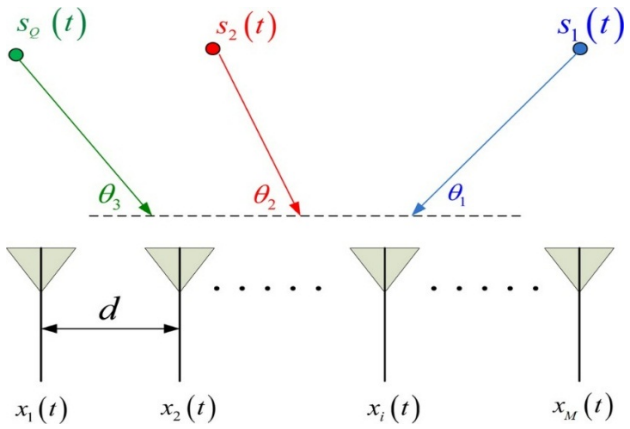

Figure 1-1 *An array sensor system with M sensors receives Q waveforms*

The problem of determining the directions-of-arrival (DOAs) of multiple narrowband plane waves using sensor arrays has received significant attention in the array signal processing literature. In practice, the estimation is made difficult by the fact that there are usually an unknown number of signals impinging on the array simultaneously, each from an unknown direction with an unknown amplitude. Furthermore, the received signals are always corrupted by noise. Nevertheless, many direction-finding approaches have been presented to solve the problem in recent years. The most commonly used among these techniques are conventional beamformer, Minimum Variance Distortion-less Response (MVDR), maximum likelihood (ML), Multiple Signal Classification (MUSIC) and Estimation of Signal Parameters via Rotational Invariance Technique (ESPRIT). The idea behind the conventional beamformer is to scan across the angular region of interest and

whichever direction produces the largest output power is the estimate of the desired signal's direction. ML employs a wavenumber window whose shape, and thus side-lobe structure, changes and is a function of the wavenumber at which an estimate is obtained [6]. Capon minimum variance method is a beamforming technique with the aim of improving the performance of conventional methods. This method reduces the influence of interference by minimizing the total output power. MUSIC is a member of a class of methods based upon the decomposition of covariance data into eigenvectors and eigenvalues. The underlying assumption behind the MUSIC algorithm is that the number of emitters seen by the receiver is less than the number of antenna elements. Under this condition, the covariance matrix of the received signal is non-singular [7] [8]. ESPRIT relies on finding the underlying rotation between the common subspaces associated with an array of pairwise-matched and codirectional sensor doublets [9] [10].

There are some other approaches which are based on Fast Fourier Transform. In [11] an algorithm for fast DOA estimation in single-channel antenna array is proposed in which the spatial Fast Fourier Transform for a multi-channel antenna array is applied to single channel antenna array. In [12] an adaptive 2-dimensional direction-finding framework is proposed to track multiple moving targets for arbitrary array structures by using the manifold separation technique. In [13], based on Fast Fourier Transform of the sensor array output data, a relationship between the FFT spectrum and the direction of arrival angles is established. In [13]**,** however, the effect of noise was neglected, and it was assumed that a large number of sensors are available.

Each method has some advantages and disadvantages compared to other algorithms. In a detailed evaluation based on thousands of simulations, the Massachusetts Institute of Technology's Lincoln Laboratory concluded that, among currently accepted high-resolution algorithms, MUSIC was the most promising and a leading candidate for further study and actual hardware implementation [14].

However, this study was done in 1998 and is true based on technology and hardware that were available in that time and it might not be valid with today modern technologies. In addition, although the performance advantages of MUSIC are substantial, they are achieved at a considerable cost in computation and storage. Furthermore, MUSIC is associated with some drawbacks like requiring relatively a large number of snapshots, sensitivity to array imperfections [15] and inability in dealing with correlated signals.

1.2 Contributions of the Thesis

The purpose of this thesis is to assess different Direction-of-Arrival estimation techniques. In this regard some popular narrow band DOA estimation methods, as well as the method proposed in [13], which is based on the spatial DFT, are reviewed and their performance is analyzed. In addition, the algorithm introduced in [13] is extended in such a way to cope with noise and its performance is analyzed for low number of sensors. In chapter 3 it is shown that the revised algorithm can lead to accurate results even in the presence of noise. Furthermore, the conditions that have to be satisfied for an accurate estimation of DOA with a low number of sensors was analyzed.

Furthermore, we prove that in the spatial DFT method, the energy of the main-lobe in the DFT spectrum is much higher than that of the side-lobes and hence, one can often ignore the effect of the side-lobes. This in turn leads the peaks of the spectrum associated with a DOA to become distinguishable.

Another contribution of the thesis is the comparison which is carried out between different algorithms to pinpoint advantages and disadvantages of each algorithm. The effect of various

parameters like number of sensors, number of snapshots and noise on the performance of algorithms are also investigated. It is illustrated that the spatial DFT method gives good results with few snapshots, can handle noise and gives satisfactory results when few sensors are available.

1.3 Thesis Organization

This thesis consists of four sections and organized as follow: in chapter two, an overview of an array antenna system will be outlined and a model for the received signal at the antenna will be presented. Then we continue with a brief review of various DOA estimation algorithms and provide a background about some of the most commonly used methods.

In chapter three we present a new approach based on the spatial FFT algorithm introduced in [13] and extend its analysis to high noise cases. Furthermore, the effects of the number of sensors on the accuracy of the DOA estimation is investigated. It is indicated that an accurate DOA estimation can be obtained with a low number of sensors.

Simulation results are presented in chapter four, where the introduced method is compared in terms of resolution, noise robustness, inter element spacing and snapshot effect against the most widely used DOA estimation algorithms. It is shown that the proposed algorithm has a good performance regarding having a small number of snapshots, small number of sensors, high resolution and noisy environment. The analysis is based on Uniform Linear Array (ULA) antennas.

Finally, in chapter five, concluding remarks and suggestions for future work are presented.

Chapter 2

An Introduction to DOA Estimation

2.1 Introduction

First, a mathematical model for received signal at an array antenna will be obtained. In this regard, the most common array antenna, the Uniform Linear Array, will be introduced. Then some of the most commonly used DOA estimation algorithms are reviewed and their advantages or disadvantages will be outlined. We divide them into two main categories; subspace methods and non-subspace methods. Some of these algorithms have been expanded over that past few years and several modified methods have been introduced. In this section, however, we just review the original works.

2.2 Uniform Linear Array and received signal model

Consider an M-element uniformly spaced linear array which is illustrated in Figure 2-1. In Figure 2-1, the array elements are equally spaced by a distance *d*, and a plane wave arrives at the array from a direction θ off the array broadside. The angle θ is called the direction-of-arrival (DOA) or angle-of-arrival (AOA) of the received signal and is measured clockwise from the broadside of the array.

Consider the signal to be the complex sinusoidal signal which is represented in complex from as, $e^{i\omega_0 t}$. The signal received by the reference element antenna is given by

$$s_1(t) = e^{j2\pi f_0 t} \tag{2-1}$$

From the Figure 2-1, the received signal by the second element of the array antenna will be the delayed version of the signal received by the first element. Consider the occurred delay is τ. Hence, the signal at the second element is given by

$$s_2(t) = s_1(t-\tau) = e^{j2\pi f_0 t} \,.\, e^{-j2\pi f_0 \tau} \tag{2-2}$$

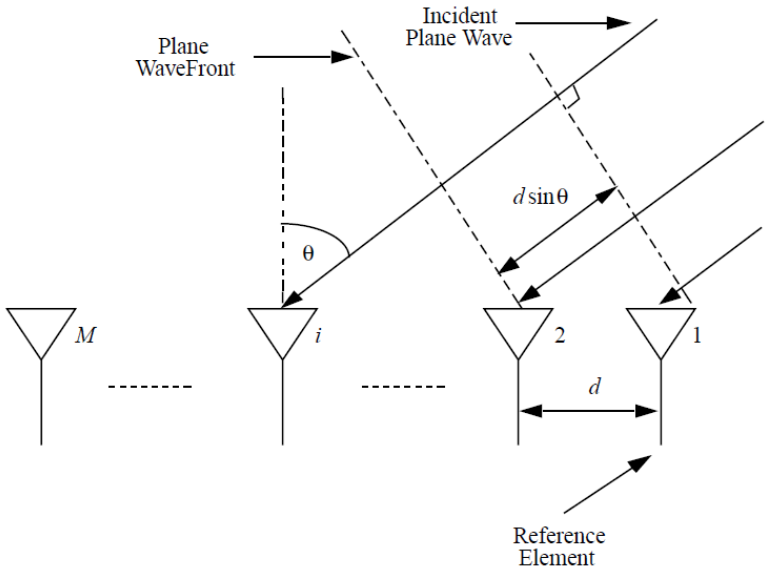

Figure 2-1 *Illustration of a plane wave incident on a Uniformly Spaced Linear Array Antenna from direction Θ*

Delay time, τ is given by

$$\tau = \frac{d\sin\theta}{c} = \frac{d\sin\theta}{f_0\lambda_0} \tag{2-3}$$

On substituting equation (2-3) in equation (2-2), we get

$$\begin{aligned} s_2(t) &= e^{j2\pi f_0 t} \,.\, e^{-j2\pi f_0 \frac{d\sin\theta}{f_0\lambda_0}} \\ &= e^{j2\pi f_0 t} \,.\, e^{-j2\pi \frac{d\sin\theta}{\lambda_0}} \end{aligned} \tag{2-4}$$

$$= e^{j2\pi f_0 t} \cdot e^{-j\emptyset}$$

where

$$\emptyset = 2\pi \frac{d \sin\theta}{\lambda_0} \tag{2-5}$$

Therefore

$$s_2(t) = s_1(t)e^{-j\emptyset} \tag{2-6}$$

The total signals received by the array antenna elements are

$$\begin{aligned} x_1(t) &= s_1(t) + n_1(t) \\ x_2(t) &= s_1(t-\tau) + n_2(t) \\ &\vdots \end{aligned} \tag{2-7}$$

In vector form it could be represented as:

$$\begin{bmatrix} x_1(t) \\ x_2(t) \\ \vdots \\ x_M(t) \end{bmatrix} = \mathbf{S}(t) \begin{bmatrix} 1 \\ e^{-j\emptyset} \\ e^{-j2\emptyset} \\ \vdots \\ e^{-j(M-1)\emptyset} \end{bmatrix} + \begin{bmatrix} n_1(t) \\ n_2(t) \\ \vdots \\ n_M(t) \end{bmatrix} \tag{2-8}$$

In which $\mathbf{S}(t)$ is a diagonal matrix with s_1 on its main diagonal. If we have '*Q*' narrowband sources with known center frequency, f_0, and directions: Θ_1 , Θ_2, … , Θ_Q impinging on the *M* -element array, the array output can be expressed as

$$\boldsymbol{x}(t) = \sum_{k=1}^{Q} \boldsymbol{a}(\emptyset_k) s_k(t) + \boldsymbol{n}(t) \tag{2-9}$$

where,

1. $\boldsymbol{x}(t) = [x_1(t) \quad ... \quad x_M(t)]^T$ is the vector of signals received by the antenna array.

2. $s_k(t)$, is the signal emitted by the k^{th} source as received at the reference sensor 1 of the array.
3. $\boldsymbol{a}(\emptyset_k) = [1 \quad e^{-j(\emptyset_k)} \quad \dots \quad e^{-j(M-1)(\emptyset_k)}]^T$, is the steering vector of the array towards the direction $\emptyset_k$
4. $i(\emptyset_k)$, is the propagation delay between the first and the i^{th} sensor for a waveform coming from the direction $\emptyset_k$
5. $\boldsymbol{n}(t) = [n_1(t) \quad \dots \quad n_M(t)]^T$, is the noise vector.

Now after obtaining a model for received signals, this section describes some common methods for the DOA estimation. We divide them into two general categories: subspace techniques and non-subspace techniques.

2.3 Non-Subspace Techniques

These methods depend on the spatial spectrum, and DOAs are obtained as locations of peaks in the spectrum. These methods are conceptually simple but offer modest or poor performance in terms of resolution. One of the main advantages of these techniques is that they can be used in situations where we lack information about the properties of the signals.

2.3.1 Delay-And-Sum Method

The delay-and-sum method also referred to as the classical beamformer method or Bartlett method [16], [17], is one of the simplest techniques for DOA estimation. Figure 2-2, shows the classical narrowband beamformer structure, where the output signal *y(k)* is given by a linearly weighted sum of the sensor element outputs. That is,

$$y(k) = \boldsymbol{w}^H \boldsymbol{u} \tag{2-10}$$

where $\boldsymbol{u}$ is the vector of the sensors' output $\boldsymbol{u} = [u_1, u_2, \cdots, u_M]$

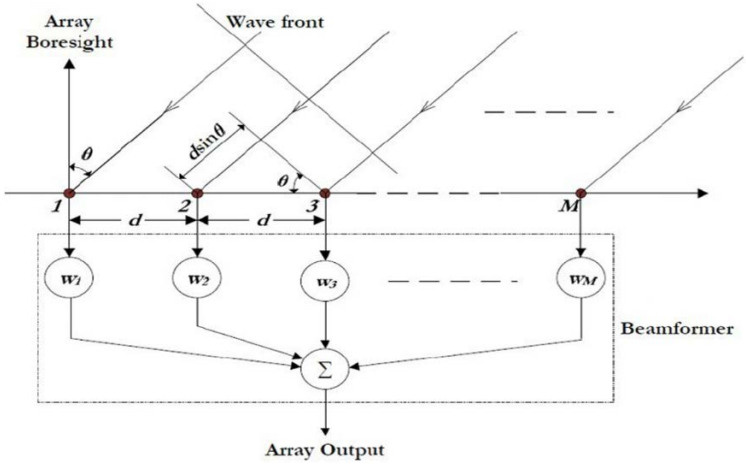

Figure 2-2. *Classical narrowband beam-former*

The idea is to scan across the angular region of interest (usually in discrete steps), and whichever direction produces the largest output power is the estimate of the desired signal's direction. More specifically, as the look direction θ is varied incrementally across the space of access, the array response vector $\boldsymbol{a}(\emptyset_k)$ and received signal autocovariance matrix $\boldsymbol{R}_{xx}$ are calculated and the output power of the beamformer is measured by

$$P_{CBF}(\emptyset) = \frac{\boldsymbol{a}^H(\emptyset)\mathbf{R}_{xx}\boldsymbol{a}(\emptyset)}{\boldsymbol{a}^H(\emptyset)\boldsymbol{a}(\emptyset)} \tag{2-11}$$

This is also referred to as the spatial spectrum and the estimate of the true DOA is the angle θ that corresponds to the peak value of the output power spectrum. The poor resolution is a significant weakness of the method [16], [17]. Delay and sum method, however, is the base tool in many newer methods such as [18] [19] [20].

2.3.2 Capon's Minimum Variance Technique

The delay-and-sum method works on the premise that pointing the strongest beam in a particular direction yields the best estimate of power arriving in that direction. Capon's minimum variance method [6] , also known as the Minimum Variance Distortion-less Response (MVDR), is an attempt to overcome the poor resolution problem associated with the delay-and-sum method and it results in a significant improvement. Several improvements and modifications to this method were presented in [21] [22] [23] [24]. In this method the output power is minimized with the constraint that the gain in the desired direction remains unity. Solving this constraint optimization problem for the weight vector we obtain

$$\boldsymbol{w} = \frac{\mathbf{R}_{xx}^{-1}\boldsymbol{a}(\emptyset)}{\boldsymbol{a}^{H}(\emptyset)\mathbf{R}_{xx}^{-1}\boldsymbol{a}(\emptyset)} \tag{2-12}$$

And output power is given by Capon's spatial spectrum

$$P_{capon} = \frac{1}{\boldsymbol{a}^{H}(\emptyset)\mathbf{R}_{xx}^{-1}\boldsymbol{a}(\emptyset)} \tag{2-13}$$

The MVDR requires an additional matrix inversion compared to the conventional beamforming method and it exhibits greater resolution than conventional beamformer in most cases. But since this algorithm is based upon covariance matrix inversion, it suffers in the presence of source correlation. If the sources are highly correlated they cannot be separated. Also, below a specific threshold SNR, the performance of Capon algorithm degrades swiftly.

2.3.3 Maximum Likelihood Technique

Maximum likelihood estimation seeks the parameter values that are most likely to have produced the observed distribution. Maximum likelihood (ML) techniques [25] [26] [27] [28] were some of

the first techniques investigated for DOA estimation. Since ML techniques were computationally intensive, they are less popular than other techniques. However, in terms of performance, they are superior to other estimators, especially at low SNR conditions [29]. Moreover, unlike subspace-based techniques they can also perform well in correlated signal conditions. Maximum Likelihood (ML) direction-of-arrival (DOA) estimation techniques play an important role in sensor array processing because they provide an excellent asymptotic DOA estimation in presence of high noise [30], [31], [32]. One of the key assumptions used in formulation of both the deterministic and stochastic ML estimators [31] is the so-called spatially homogeneous white noise assumption. In general, the ML approach is optimal in the maximum likelihood sense.

Besides its advantages, there are also some limitations associated with this method which make it an impractical algorithm. For example, the algorithm assumes knowledge of the interference covariance matrix, something that may not be available or difficult to accurately estimate in practice. Also, the maximization of the log-likelihood function is a nonlinear optimization problem that requires multidimensional search and thus the algorithm is computationally intensive.

2.4 Subspace Techniques

Subspace-based methods depend on observations concerning the eigendecomposition of the covariance matrix into a signal subspace and a noise subspace. Two of these methods MUSIC and ESPRIT are briefly reviewed here.

2.4.1 MUSIC Algorithm

MUSIC stands for Multiple Signal Classification [8]. It is one of the earliest proposed and a very popular method for high-resolution direction finding. Basic idea behind the MUSIC algorithm is to separate the signal from noise by using the orthogonality property of their spaces through eigendecomposition of the correlation matrix of the received signal. It provides information about direction of arrival (DOA) of each signal and the number of incident signals [33]. Several modified and improved algorithms based on MUSIC algorithm have been presented [34] [35] [36] [37] [38]. MUSIC, like many adaptive techniques, is dependent on the correlation matrix of the data. MUSIC is a technique based on exploiting the eigenstructure of the input covariance matrix. Eigenvectors are easily obtained by either an eigen decomposition of the sample covariance matrix or a Singular Value Decomposition (SVD) of the data matrix [8], [39]

If there are *Q* signals incident on the array, the received input data vector at an *M*-element array can be expressed as a linear combination of the incident waveforms and noise. As in equation (2-9),

$$\boldsymbol{x}(t) = \sum_{q=0}^{Q-1} \boldsymbol{a}(\emptyset_q) s_q(t) + \boldsymbol{n}(t) \tag{2-14}$$

$$\begin{aligned} \boldsymbol{x}(t) &= \begin{bmatrix} \boldsymbol{a}(\emptyset_0) & \boldsymbol{a}(\emptyset_1) & \cdots & \boldsymbol{a}(\emptyset_{Q-1}) \end{bmatrix} \begin{bmatrix} s_0(t) \\ s_1(t) \\ \vdots \\ s_{Q-1}(t) \end{bmatrix} + \boldsymbol{n}(t) \\ &= \mathbf{A}\boldsymbol{s}(t) + \boldsymbol{n}(t) \end{aligned} \tag{2-15}$$

Where $\boldsymbol{s}^T(t) = [s_0(t) \quad s_1(t) \quad \cdots \quad s_{Q-1}(t)]$ is the vector of incident signals, $\boldsymbol{n}(t) = [n_0(t) \quad n_1(t) \quad \cdots \quad n_{Q-1}(t)]$ is the noise vector, and $\boldsymbol{a}(\emptyset_q)$ is the array steering vector corresponding to the Direction-Of-Arrival of the q^{th} signal.

In geometric terms, the received vector $\boldsymbol{x}(t)$ and the steering vectors $\boldsymbol{a}(\emptyset_q)$ can be visualized as vectors in *M*-dimensional space. From equation (2-15), it is seen that the received vector $\boldsymbol{x}(t)$ is a particular linear combination of the array steering vectors, with $s_0(t) \quad s_1(t) \quad \cdots \quad s_{Q-1}(t)$ being the coefficients of the combination. In terms of the above data model, the input covariance matrix $\mathbf{R}_{xx}$ can be expressed as

$$\mathbf{R}_{xx} = E[\boldsymbol{x}\boldsymbol{x}^H] = \mathbf{A}\, E[\boldsymbol{s}\boldsymbol{s}^H]\, \mathbf{A}^H + E[\boldsymbol{n}\boldsymbol{n}^H] \tag{2-16}$$

$$\mathbf{R}_{xx} = \mathbf{A}\, \boldsymbol{R}_{ss}\, \mathbf{A}^H + \sigma_n^2 \mathbf{I} \tag{2-17}$$

where $\mathbf{R}_{ss}$, is the signal correlation matrix $E[\boldsymbol{s}\boldsymbol{s}^H]$.

The eigenvalues of $\mathbf{R}_{xx}$ are the values, $\{\lambda_0 \quad \cdots \quad \lambda_{M-1}\}$ such that

$$|\mathbf{R}_{xx} - \lambda_i \mathbf{I}| = 0 \qquad i = 0, \cdots, M-1 \tag{2-18}$$

Using (2-17), we can rewrite this as

$$|\mathbf{A}\, \mathbf{R}_{ss}\, \mathbf{A}^H + \sigma_n^2 \mathbf{I} - \lambda_i \mathbf{I}\,| = |\mathbf{A}\, \mathbf{R}_{ss}\, \mathbf{A}^H - (\lambda_i - \sigma_n^2)\mathbf{I}\,| = 0 \qquad i = 0, \cdots, M-1 \tag{2-19}$$

Therefore, the eigenvalues β_i of $\mathbf{A}\, \mathbf{R}_{ss}\, \mathbf{A}^H$ are

$$\beta_i = \lambda_i - \sigma_n^2 \quad ; \quad i = 0, \cdots, M-1 \tag{2-20}$$

Since **A** is comprised of steering vectors which are linearly independent, it has full column rank, and the signal correlation matrix $\mathbf{R}_{ss}$ is non-singular as the incident signals are assumed to be uncorrelated.

A full column rank **A** matrix and non-singular $\mathbf{R}_{ss}$ guarantee that, when the number of incident signals, *Q*, is less than the number of array elements *M*, the $M \times M$ matrix $\mathbf{A}\,\mathbf{R}_{ss}\,\mathbf{A}^H$ is positive semidefinite with rank *Q*.

From elementary linear algebra, this implies that $M - Q$ of the eigenvalues, β_i , of $\mathbf{A}\,\mathbf{R}_{ss}\,\mathbf{A}^H$ are zero. From equation (2-20), this means that $M - Q$ of the eigenvalues of $\mathbf{R}_{xx}$ are equal to the noise variance, σ_n^2 . We then sort the eigenvalues of $\mathbf{R}_{xx}$ such that λ_0 is the largest eigenvalue, and λ_{M-1} is the smallest eigenvalue. Therefore,

$$\lambda_i = \sigma_n^2 \quad ; \quad i = Q, \cdots, M-1 \tag{2-21}$$

In practice, however, when the autocorrelation matrix $\mathbf{R}_{xx}$ is estimated from a finite data sample, all the eigenvalues corresponding to the noise power will not be identical. Instead they will appear as a closely spaced cluster, with the variance of their spread decreasing as the number of samples used to obtain an estimate of $\mathbf{R}_{xx}$ is increased. Once the multiplicity, *K*, of the smallest eigenvalue is determined, an estimate of the number of signals, $\hat{Q}$, can be obtained from relation $M = Q + K$. Therefore, the estimated number of signals is given by

$$\hat{Q} = M - K \tag{2-22}$$

The eigenvector associated with a particular eigenvalue, λ_i is the vector $\boldsymbol{v}_i$ such that

$$(\mathbf{R}_{xx} - \lambda_i \mathbf{I})\boldsymbol{v}_i = 0 \quad ; \quad i = 0, \cdots, M-1 \tag{2-23}$$

For eigenvectors associated with $M - Q$ smallest eigenvalues, we have

$$(\mathbf{R}_{xx} - \sigma_n^2\mathbf{I})\boldsymbol{v}_i = \mathbf{A}\,\mathbf{R}_{ss}\,\mathbf{A}^H\boldsymbol{v}_i + \sigma_n^2\mathbf{I}\boldsymbol{v}_i - \sigma_n^2\mathbf{I}\boldsymbol{v}_i = 0$$
$$i = Q, Q+1, \cdots, M-1 \tag{2-24}$$

$$\mathbf{A}\,\mathbf{R}_{ss}\,\mathbf{A}^H\boldsymbol{v}_i = 0 \quad ; \quad i = Q, Q+1, \cdots, M-1 \tag{2-25}$$

Since $\mathbf{A}$ has full rank and $\mathbf{R}_{ss}$ is non-singular, this implies that

$$\mathbf{A}^H\boldsymbol{v}_i = 0$$
$$\begin{bmatrix} \boldsymbol{a}^H(\emptyset_0)\boldsymbol{v}_i \\ \boldsymbol{a}^H(\emptyset_1)\boldsymbol{v}_i \\ \vdots \\ \boldsymbol{a}^H(\emptyset_{Q-1})\boldsymbol{v}_i \end{bmatrix} = \begin{bmatrix} 0 \\ 0 \\ \vdots \\ 0 \end{bmatrix} \tag{2-26}$$
$$i = Q, Q+1, \cdots, M-1$$

This means that the eigenvectors associated with the $M - Q$ smallest eigenvalues are orthogonal to the Q steering vectors that make up $\mathbf{A}$.

$$\{\boldsymbol{a}(\emptyset_0) \quad \boldsymbol{a}(\emptyset_1) \quad \cdots \quad \boldsymbol{a}(\emptyset_{Q-1})\} \perp \{\boldsymbol{v}_Q \quad \cdots \quad \boldsymbol{v}_{M-1}\} \tag{2-27}$$

This is the essential observation of the MUSIC approach. It means that one can estimate the steering vectors associated with the received signals by finding the steering vectors which are most nearly orthogonal to the eigenvectors associated with the eigenvalues of $\mathbf{R}_{xx}$ that are approximately equal to σ_n^2 . This analysis shows that the eigenvectors of the covariance matrix $\mathbf{R}_{xx}$ belong to either of the two orthogonal subspaces, called the principle eigen subspace (signal subspace) and the non-principle eigen subspace (noise subspace) [8]. The steering vectors corresponding to the Direction-Of-Arrival lie in the signal subspace and are hence orthogonal to the noise subspace. By searching through all possible array steering vectors to find those which

are perpendicular to the space spanned by the non-principle eigenvectors, the DOA's $\emptyset$'s can be determined. To search the noise subspace, we form a matrix containing the noise eigenvectors:

$$\mathbf{V}_n = [\boldsymbol{v}_Q \quad \boldsymbol{v}_{Q+1} \quad \cdots \quad \boldsymbol{v}_{M-1}] \tag{2-28}$$

Since the steering vectors corresponding to signal components are orthogonal to the noise subspace eigenvectors, it follows that $\boldsymbol{a}^H(\emptyset)\,\mathbf{V}_n\,\mathbf{V}_n^H\,\boldsymbol{a}(\emptyset) = 0$ for $\emptyset$ corresponding to the DOA of a signal component. Then the DOAs of the incident signals can be estimated by locating the peaks of a MUSIC spatial spectrum given by,

$$P_{MUSIC}(\emptyset) = \frac{1}{\boldsymbol{a}^H(\emptyset)\,\mathbf{V}_n\,\mathbf{V}_n^H\,\boldsymbol{a}(\emptyset)} \tag{2-29}$$

or alternatively

$$P_{MUSIC}(\emptyset) = \frac{\boldsymbol{a}^H(\emptyset)\;\boldsymbol{a}(\emptyset)}{\boldsymbol{a}^H(\emptyset)\,\mathbf{V}_n\,\mathbf{V}_n^H\,\boldsymbol{a}(\emptyset)} \tag{2-30}$$

Orthogonality between $\boldsymbol{a}(\emptyset)$ and $\mathbf{V}_n$ will minimize the denominator and hence will give rise to peaks in the MUSIC spectrum defined in equation (2-29) and (2-30). The $\hat{Q}$ largest peaks in the MUSIC spectrum correspond to the signals impinging on the array.

Although the performance of MUSIC algorithm is substantial, it is achieved at a considerable cost in computation and storage (of array calibration data). Furthermore, in either low SNR scenarios or closely spaced sources (i.e., multiple peaks observed in the measurements) MUSIC's performance reduces dramatically [16], [17]. The maximum number of DOAs detectable, i.e., the capacity of DOA estimation technique, is equal to the rank of the reciprocal subspace of the selected noise subspace. Thus, the capacity of DOA estimation using MUSIC is no more than $M -$

1 where M is the number of antenna elements in the antenna array [40]. In [41], the authors prove that one requires at least N snapshots where $N > 2M$ so that the signal-to-noise ratio is within 3dB of the optimum

Also, the MUSIC algorithm fails when it comes to detecting correlated input signals. Because the covariance matrix $\mathbf{R}_{xx}$ does not satisfy the full rank condition required by the MUSIC for Eigen decomposition. Figure 2-3 shows the MUSIC spectrum for a DOA estimation problem where five correlated sources are impinging on a 20 elements array. SNR is 20dB and 25 snapshots were used. It can be observed from Figure 2-3 that the response of MUSIC algorithm is not sharp at the peaks and it fails to estimate DOA of sources. The three largest eigenvalues of covariance matrix in this example are: 2.8×10^4, 8.75×10^3 and 11×10^{-4}. The rest of eigenvalues are very smaller, in order of 10^{-14}. Therefore, covariance matrix $\mathbf{R}_{xx}$ is very close to singular matrix and does not satisfy the full rank condition required by the MUSIC algorithm.

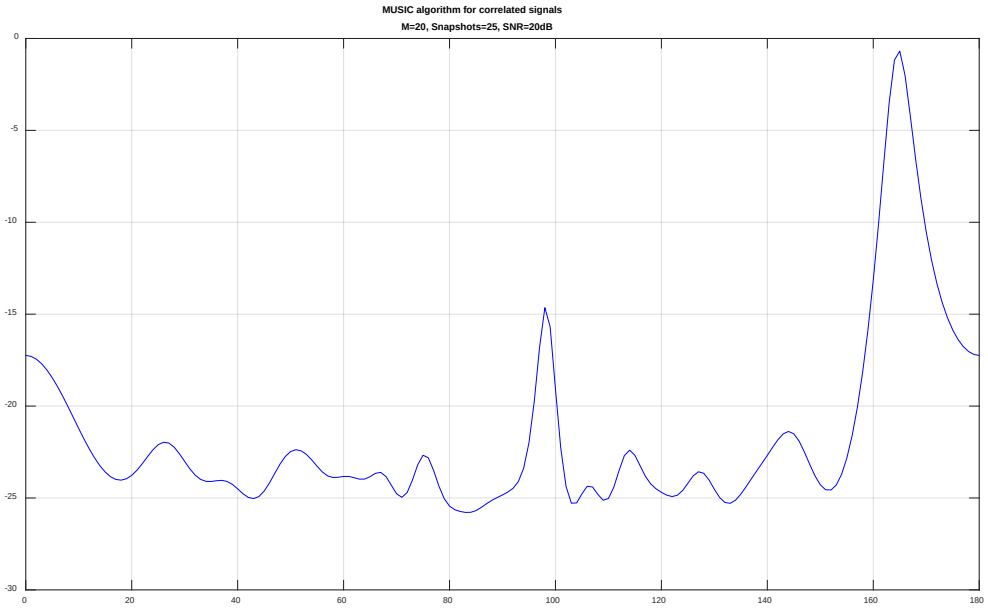

Figure 2-3. *MUSIC spectrum for five correlated signals arrive at a 20-elements array.*

2.4.2 ESPRIT Algorithm

A new approach to the signal parameter estimation problem, called ESPRIT, was proposed in [42] [15]. ESPRIT stands for Estimation of Signal Parameter via Rotational Invariance Technique and is similar to MUSIC in that it exploits the underlying data model and generates estimates that are asymptotically unbiased and efficient. In addition, it has several important advantages over MUSIC [42].

The algorithm does not require knowledge of the array geometry and element characteristics; thus, array calibration is not required, eliminating the need for the associated storage of the array manifold [42]. This algorithm is more robust with respect to array imperfections than MUSIC. Also, computational complexity and storage requirements are lower than MUSIC as it does not involve extensive search throughout all possible steering vectors [15]. But, it explores the rotational invariance property in the signal subspace created by two sub arrays derived from original array with a translation invariance structure. Unlike MUSIC, ESPRIT does not require that array manifold vectors be precisely known, hence the array calibration requirements are not stringent. The array is decomposed into two equal-sized identical subarrays with the corresponding elements of the two sub arrays displaced from each other by a fixed translational (not rotational) distance [29].

Consider an antenna array with M elements and Q signals incident on the array. Suppose that $Q < M$ and let $z_q = e^{-j2\pi\frac{d\sin\theta}{\lambda}}$, the $M \times Q$ matrix of steering vectors is given by

$$\mathbf{Str} = \begin{bmatrix} 1 & 1 & \cdots & 1 \\ z_1 & z_2 & \cdots & z_Q \\ \vdots & \vdots & \ddots & \vdots \\ z_1^{M-2} & z_2^{M-2} & \cdots & z_Q^{M-2} \\ z_1^{M-1} & z_2^{M-1} & \cdots & z_Q^{M-1} \end{bmatrix} \tag{2-31}$$

Now create a subarray with the elements 1, 2, …, $M-1$, and a subarray with elements 2, 3, ... M. Based on matrix **Str** define two $(M-1) \times Q$ matrices, $\mathbf{S}_0$ and $\mathbf{S}_1$

$$\mathbf{S}_0 = \begin{bmatrix} 1 & 1 & \cdots & 1 \\ z_1 & z_2 & \cdots & z_Q \\ \vdots & \vdots & \ddots & \vdots \\ z_1^{M-2} & z_2^{M-2} & \cdots & z_Q^{M-2} \end{bmatrix} \qquad \mathbf{S}_1 = \begin{bmatrix} z_1 & z_2 & \cdots & z_Q \\ \vdots & \vdots & \ddots & \vdots \\ z_1^{M-2} & z_2^{M-2} & \cdots & z_Q^{M-2} \\ z_1^{M-1} & z_2^{M-1} & \cdots & z_Q^{M-1} \end{bmatrix} \tag{2-32}$$

and note that $\mathbf{S}_1 = \mathbf{S}_0\mathbf{\Phi}$ where $\mathbf{\Phi}$ is the $Q \times Q$ matrix

$$\mathbf{\Phi} = \begin{bmatrix} z_1 & 0 & \cdots & 0 \\ 0 & z_2 & \cdots & 0 \\ \vdots & \vdots & \ddots & \vdots \\ 0 & 0 & \cdots & z_Q \end{bmatrix} \tag{2-33}$$

i.e., $\mathbf{\Phi}$ is a diagonal matrix whose entries correspond to the phase shift from one element to the next due to the delay for each individual signal. We see that if we can estimate $\mathbf{\Phi}$, we can estimate the DOA of all signals. If $\mathbf{S}_0$ and $\mathbf{S}_1$ were known, we could solve for $\mathbf{\Phi}$ easily. Of course, they are unknown matrices and we must use proxies to obtain the same result. The ESPRIT algorithm begins by recognizing that the steering vectors in matrix "**Str**" span the same subspace as the matrix $\mathbf{V}_s$, the $M \times Q$ matrix of signal eigenvectors. Since both these matrices span the same subspace, there exists an invertible $Q \times Q$ matrix $\mathbf{C}$ such that

$$\mathbf{V}_s = \mathbf{Str} \times \mathbf{C} \tag{2-34}$$

Defining matrices $\mathbf{V}_0$ and $\boldsymbol{V}_1$ derived from $\mathbf{V}_s$ just as $\mathbf{S}_0$ and $\mathbf{S}_1$ were derived from "**Str**", $\mathbf{V}_0$ comprises the first $(M-1)$ rows of $\mathbf{V}_s$ and $\mathbf{V}_1$ the last $(M-1)$ rows of $\mathbf{V}_s$, and using equation (2-34), we have

$$\mathbf{V}_0 = \mathbf{S}_0\mathbf{C} \tag{2-35}$$

$$\mathbf{V}_1 = \mathbf{S}_1\mathbf{C} = \mathbf{S}_0\mathbf{\Phi}\mathbf{C} \tag{2-36}$$

Consider

$$\mathbf{V}_1\mathbf{C}^{-1}\mathbf{\Phi}^{-1}\mathbf{C} = \mathbf{S}_0\mathbf{\Phi}\mathbf{C}\mathbf{C}^{-1}\mathbf{\Phi}^{-1}\mathbf{C} = \mathbf{S}_0\mathbf{C} = \mathbf{V}_0 \tag{2-37}$$

Now let

$$\boldsymbol{\psi}^{-1} = \mathbf{C}^{-1}\mathbf{\Phi}^{-1}\mathbf{C} \tag{2-38}$$

⇨ $\mathbf{V}_1\,\boldsymbol{\psi}^{-1} = \mathbf{V}_0$
⇨ $\mathbf{V}_1 = \mathbf{V}_0\,\boldsymbol{\psi}$

Where

$$\boldsymbol{\psi} = \mathbf{C}^{-1}\mathbf{\Phi}\mathbf{C} \tag{2-39}$$

Equations (2-38) and (2-33) implies that the matrix $\mathbf{\Phi}$ is a diagonal matrix of the eigenvalues of $\boldsymbol{\psi}$. Using equation (2-38) and (2-39) we now have a complete algorithm.

The steps of ESPRIT are [43]:

1. Estimate the covariance matrix of received signal, $\mathbf{R}_{xx}$, (refer to equation (2-16) and (2-17)). Find its eigendecomposition, $\mathbf{R}_{xx} = \mathbf{V}\Lambda\mathbf{V}^H$

2. Partition $\mathbf{V}$ to obtain signal subspace $\mathbf{V}_s$, corresponds to the Q largest eigenvalues of $\mathbf{V}$, which spans the signal subspace.

3. Estimate the $Q \times Q$ matrix $\boldsymbol{\psi}$ by solving the system of equations (2-38). The most commonly employed criterion for problem of obtaining suitable estimate is the *least square* criterion. The standard least square criterion applied to the model $AX=B$ to obtain an estimate of X assumes A is known and the error is to be attributed to B. Assuming the set of equations is overdetermined, the columns of A are linearly independent, and the noise in elements of B is zero mean, the LS solution is $\hat{X} = [A^H A]^{-1} A^H B$.

4. Find the eigenvalues of $\boldsymbol{\psi}$. Eigenvalues of $\boldsymbol{\psi}$ are the diagonal elements of $\boldsymbol{\Phi}$ which are the estimates of z_q that we are looking for.

5. Obtain the DOA using $\theta_q = \sin^{-1}\left(\frac{\arg(z_q)\lambda}{2\pi d}\right)$

As can be seen from the above discussion, ESPRIT eliminates the search procedure inherent in most DOA estimation methods and produces the DOA estimates directly in terms of the eigenvalues. In practice, one would obtain the estimate of $\boldsymbol{\psi}$ not using least squares, but Total Least Squares (TLS). This is an improved least squares technique introduced in [15]. Over the past decades many modified and improved algorithms based on ESPRIT technique have been presented [44] [45] [46] [47] [48] [49] [50].

2.5 Discussion and Summary of the chapter

In this chapter the Uniform Linear Array was introduced and a model for the output of array was obtained. Also, some common methods for the DOA estimation were described.

The DOA estimation method was first implemented using the conventional beamforming algorithm. Its main idea is: at each direction, make the array to measure the output power in that direction and the direction that produce maximum output power is DOA estimation [51]. The main

shortcoming of the conventional beamforming method is that: all of the degrees of freedom in the array are used to form a beam in the desired direction of observation. When multiple signal sources are incident, the method is limited by the size of the beam width and the side-lobes, so the resolution is low.

Capon minimum variance method is a beamforming technique for the purpose of enhancing the performance of conventional methods. Conventional beamforming methods have a defect: when there are multiple signal sources, the spatial spectrum estimation includes the signal source power not only in the estimation direction but also in other directions. The Capon method reduces the influence of interference by minimizing the total output power of array, and thus better estimates the direction of the wave. Compared with conventional beamforming algorithm, the Capon method has greatly improved resolution. However, the Capon method has obvious shortcomings: if the other signal's incident direction is close to the interest signal's incident direction, the Capon method will make many errors. It also needs to compute the matrix inversion and finally, the ability to distinguish is decided by the array geometry and SNR.

Then, Maximum Likelihood (ML) was reviewed. It represents an important category of DOA estimators that determine source DOAs by maximizing the loglikelihood function, which signifies that signals from those directions are most likely to cause occurrence of the given samples. ML produces relatively superior estimates compared to other methods, especially in unfavorable conditions involving low SNR, short data samples, highly correlated or coherent sources, and small array apertures. Two types of solutions have been obtained: one for the case of deterministic signals (referred to as conditional ML), and one for a stochastic signals model (referred to as unconditional ML). Despite the desirable properties of these ML estimators, they have not enjoyed much practical application since they typically require non-linear, multidimensional optimization

procedures. In the case of conditional ML, a further drawback is that its estimates do not asymptotically achieve the Cramer-Rao lower bound (the theoretical limit on how well the DOA can be estimated) on estimate variance [52]. This is due to the fact that the number of free parameters to be estimated grows with the amount of data collected.

After that, we described the MUSIC algorithm. The basic idea of MUSIC algorithm is to conduct eigenvalue decomposition for the covariance matrix of any array output data, resulting in a signal subspace corresponding to the signal components that is orthogonal to the noise subspace. Then these two orthogonal subspaces are used to constitute a spectrum function, and a spectral peak search is used to detect DOA signals. Although, MUSIC algorithm has a high resolution, accuracy and stability under certain conditions, there are some limitation as well. The MUSIC algorithm is limited to uncorrelated signals. When the source is a correlated signal, the estimated performance of the MUSIC algorithm can deteriorate completely. It also demands a great deal of computation. Another drawback is the fact that complete knowledge of the array manifold is required.

Finally, the ESPRIT technique was described. ESPRIT is another parameter estimation technique, based on the fact that in the steering vector, the signal at one element has a constant phase shift from the earlier element. The goal of the ESPRIT technique is to exploit the rotational invariance in the signal subspace which is created by two arrays with a translational invariance structure. It does not involve an exhaustive search through all possible steering vectors to estimate DOA and reduces the computational and storage requirements compared to MUSIC [15]. It is also less dependent on the array size and can perform relatively well.

Chapter 3

Spatial Discrete Fourier Transform Algorithm

3.1 Introduction

In 2002, Liang Tao and Kwan introduced a novel approach to DOA estimation technique using the Fast Fourier transform of sensor array output in the spatial dimension [13]. In [53] this algorithm with minor modification was used as part of a multistage space-time equalizer. In [13], a large number of sensors (256) were used to perform simulations and assess the performance of the algorithm. To obtain good performance, Tao and Kwan suggested to either use a large number of sensors, which may make the size of the sensor array too large, or to select a smaller wavelength of narrowband signals whenever possible. We, however, do not have control on sources and their wavelength and as a result the algorithm typically requires a large number of sensors. In addition, another contributing factor is noise which was not taken into account in the algorithms introduced in [13] and [53] where it was assumed that the noise is very low.

In this section the DOA estimation method introduced in [13] is further developed and we show that with a little modification, which will be described in section 3.3, the method is able to accurately estimate DOA in presence of high noise, even with a limited number of sensors.

This chapter is structured as follows: first we define the DOA estimation problem and obtain a model for received signal at the array at the n^{th} sample. Then in proposition 1 the approach introduced in [53] and [54] is presented in which the environment is assumed to be noise-free and an infinite number of sensors are available. A proof for this proposition is also provided. In the

next step we suppose that one of the two conditions is not true, for example, noise is not negligible and/or a limited number of sensors are available. In proposition 2 it is proved that averaging the DFT of the output over N_s snapshots provides accurate DOA estimation and the noise effect is constant over the spectrum. In proposition 3 it is shown that one can use a small number of sensors to estimate the DOA of impinging sources and two sets of assumptions are formulated that must be satisfied to avoid the overlapping of main-lobes in spectrum.

The major advantages of proposed method are as follows: the algorithm is fast and can provide a good DOA estimation using a small number of snapshots, it has improved resolution in comparison to methods like Bartlett and MUSIC and finally it is able to accurately estimate DOA in a severely noisy environment with even a limited number of sensors.

3.2 Problem Definition

Q statistically-independent narrowband sources with the common wavelength (λ) are transmitting data $(t_q(n)$, for $q = 1, 2, \dots, Q)$ to the base station with distinct direction of arrivals (DOAs) denoted by $\theta_1, \theta_2, \dots, \theta_Q$. The sequence generated by each source is independent and identically distributed (i.i.d) with zero mean. A white Gaussian model is adopted as the probability density function of the background noise. Further, the noise and all *Q* sources are independent. The goal here is to accurately estimate the DOA of all sources.

Consider an *M*-element uniform linear array with space d between elements at the base station. After sampling, the baseband received signal at the antenna at the n^{th} sample is given by:

$$\boldsymbol{x}(n) = [x_1(n) \quad x_2(n) \quad \cdots \quad x_M(n)]^T = \sum_{q=1}^{Q} t_q(n)\boldsymbol{v}_q + \boldsymbol{\eta}(\mathrm{n}) \tag{3-1}$$

where $t_q(n)$ is the signal received at the antennas from each user. Further, $\boldsymbol{\eta}(n)$ is a $M \times 1$ complex-valued white Gaussian noise vector at the n^{th} sample and $\boldsymbol{v}_q$ is the array manifold vector:

$$\begin{aligned} &\boldsymbol{\eta}(n) = [\eta_1(n) \ \eta_2(n) \ \cdots \ \eta_M(n)]^T \\ &\boldsymbol{v}_q = \left[1 \ e^{-j(\frac{2\pi}{\lambda}d)cos(\theta_q)} \ e^{-j2(\frac{2\pi}{\lambda}d)cos(\theta_q)} \ \cdots \ e^{-j(M-1)(\frac{2\pi}{\lambda}d)\cos(\theta_q)}\right]^T \end{aligned} \tag{3-2}$$

3.3 DFT-based DOA Estimation Approach

By applying a K-point discrete Fourier Transform (DFT) to $\boldsymbol{x}(n)$ (received signal at the antenna at the n^{th} temporal sample), i.e. DFT in the spatial dimension and zero-padding by adding $K - M$ zeros, we get (K is an odd number):

$$\begin{aligned} \boldsymbol{X}_{(n)}(k) &= \sum_{i=0}^{K-1} \boldsymbol{x}_i(n)e^{-j\frac{2\pi}{K}ik} + \sum_{i=0}^{K-1} \eta_i(n)e^{-j\frac{2\pi}{K}ik} \\ &= \sum_{i=0}^{M-1}\left(\sum_{q=1}^{Q} t_q(n)e^{-j(\frac{2\pi}{\lambda}d)\cos(\theta_q)i}\right)e^{-j\frac{2\pi}{K}ik} + \sum_{i=0}^{M-1} \eta_i(n)e^{-j\frac{2\pi}{K}ik} \\ &\sum_{q=1}^{Q} t_q(n)\left(\sum_{i=0}^{M-1} e^{-j\left(\left(\frac{2\pi}{\lambda}d\right)\cos(\theta_q)+\frac{2\pi}{K}k\right)i}\right) + \sum_{i=0}^{M-1} \eta_i(n)e^{-j\frac{2\pi}{K}ik} \qquad for \quad -l \le k \le l \end{aligned} \tag{3-3}$$

where $l = \frac{K-1}{2}$

In the second line of the above derivation, $K-1$ in sigma can be replaced by $M-1$ because of zero terms. In fact, the effect of zero-padding by $K-M$ is to provide a better frequency resolution ($2\pi/K$). It can be shown that equation (3-3) can be represented in the following form [1]:

$$\boldsymbol{X}_{(n)}(k)=\sum_{q=1}^{Q} t_q(n)\frac{sin\left(\frac{\pi d\ cos(\theta_q)}{\lambda}+\frac{\pi k}{K}\right)M}{sin\left(\frac{\pi d\ cos(\theta_q)}{\lambda}+\frac{\pi k}{K}\right)}e^{-j\left(\left(\frac{2\pi}{\lambda}d\right)\cos(\theta_q)+\frac{2\pi k}{K}\right)\left(\frac{M-1}{2}\right)}+\boldsymbol{\Psi}_{(n)}(k) \tag{3-4}$$

where:

$$\boldsymbol{\Psi}_{(n)}(k)=\sum_{i=0}^{M-1}\eta_i(n)e^{-j\frac{2\pi}{K}ik} \tag{3-5}$$

Proposition 1 [53]: For a noise-free environment, when the number of sensors *M* goes to infinity the locations of the *Q* largest peaks of $\left|\boldsymbol{X}_{(n)}(k)\right|^2$ denoted by $k_q\ ; q=1,2,\dots,Q$ can provide an asymptotically consistent estimate of DOAs given by:

$$\hat{\theta}_q=acos\left(-\frac{k_q\,\lambda}{Kd}\right)\qquad for\ q=1,2,\dots,Q \tag{3-6}$$

Proof: Consider the following function:

$$\Gamma\left(\Theta_q\right)=\frac{\sin(\Theta_q M)}{\sin(\Theta_q)} \tag{3-7}$$

where $\Theta_q=\left(\frac{\pi d\ cos(\theta_q)}{\lambda}+\frac{\pi k}{K}\right)$

When M approaches to infinity $\Gamma\left(\Theta_q\right)$ can be approximated as:

$$\Gamma\left(\Theta_q\right)=M\delta(\Theta_q) \tag{3-8}$$

By replacing equation (3-8) into equation (3-4) (assuming the environment is noise-free):

$$\boldsymbol{X}_{(n)}(k) = \sum_{q=1}^{Q} t_q(n) M\delta\left(\frac{\pi d\ cos(\theta_q)}{\lambda} + \frac{\pi k}{K}\right) e^{-j\left(\left(\frac{2\pi}{\lambda}d\right)cos(\theta_q)+\frac{2\pi k}{K}\right)\left(\frac{M-1}{2}\right)} \tag{3-9}$$

Using the Sifting property of the delta function, equation (3-9) can be expressed as:

$$\boldsymbol{X}_{(n)}(k) = \sum_{q=1}^{Q} t_q(n) M\delta\left(\frac{\pi d\ cos(\theta_q)}{\lambda} + \frac{\pi k}{K}\right) \tag{3-10}$$

Since each of Q delta functions is non-zero at a distinct k_q, we get:

$$\left|\boldsymbol{X}_{(n)}(k)\right|^2 = \left|\sum_{q=1}^{Q} t_q(n) M\delta\left(\frac{\pi d\ cos(\theta_q)}{\lambda} + \frac{\pi k}{K}\right)\right|^2 = M^2 \sum_{q=1}^{Q} \left|t_q(n)\right|^2 \left|\delta\left(\frac{\pi d\ cos(\theta_q)}{\lambda} + \frac{\pi k}{K}\right)\right|^2 \tag{3-11}$$

Equation (3-11) implies that there are exactly Q distinct peaks, each of which is corresponding to the DOA of q^{th} user given by equation (3-6).

■

Expressing equation (3-7) as (3-8) implies that the accuracy of DOA estimation technique increases as the number of sensors (and accordingly the aperture size) is increasing, which is a well-known result from the literature [1] [13] [16] [17] [29]. In the following section, it will be shown that with a small modification the DFT-based DOA estimation approach is able to accurately estimate DOA in a severely noisy environment even with a limited number of sensors. In this regard, we proposed to take average on the peaks of the DFTs, $\boldsymbol{X}_n(k)$, obtained from a sequence of N_s snapshots. As will be discussed in proposition 3, the estimated DOAs are

corresponding to the maxima of $E\left\{\left|\boldsymbol{X}_{(n)}(k)\right|^2\right\}$. In practice, in order to estimate the expected value of $\left|\boldsymbol{X}_{(n)}(k)\right|^2$, the *K*-point DFT needs to be applied to N_s subsequent snapshots ($n = 1, 2, \cdots, N_s$). With N_s sufficiently large, the average over N_s approaches $E\left\{\left|\boldsymbol{X}_{(n)}(k)\right|^2\right\}$. First, we need to obtain the expected value of $\left|\boldsymbol{X}_{(n)}(k)\right|^2$ over time index (n).

Proposition 2 [54]**:** The expected value of $\left|\boldsymbol{X}_{(n)}(k)\right|^2$ over time index (n) can be expressed as:

$$E\left\{\left|\boldsymbol{X}_{(n)}(k)\right|^2\right\} = \Gamma_1(k) + 2M\sigma^2 \qquad for \qquad -l \le k \le l \tag{3-12}$$

where

$$\Gamma_1(k) = \sum_{q=1}^{Q} \zeta_q \left(\frac{\sin\left(\left(\frac{\pi d \cos(\theta_q)}{\lambda} + \frac{\pi k}{K}\right) M\right)}{\sin\left(\frac{\pi d \cos(\theta_q)}{\lambda} + \frac{\pi k}{K}\right)} \right)^2 \tag{3-13}$$

$$\sigma^2 = E[\,(\mathrm{Re}\,\{\eta_i(n)\}\,)^2\,] = E[\,(\mathrm{Im}\,\{\eta_i(n)\}\,)^2\,]$$
$$\zeta_q = E\left|t_q(n)\right|^2 \tag{3-14}$$

The proof of proposition 2 can be found in appendix A.

Proposition 2 indicates that the noise effect is constant over $-l \le k \le l$. Thus, it can be concluded that in theory (even severe) noise has no destructive effect on the estimated DOAs.

Proposition 3 [54]**:** The Q peak locations of the expected value of $\left|\boldsymbol{X}_{(n)}(k)\right|^2$ denoted by $k_1, k_2, \ldots, k_Q$ can provide an asymptotically consistent estimate of DOAs given by equation (3-6) if:

Assumption 1: If $\theta_1 \le \theta_2 \le \cdots \le \theta_Q$ then $\Psi \ge \frac{2\lambda}{Md}$ where Ψ is the minimum value of all possible cases for $\cos\theta_i - \cos\theta_{i+1}$; $(i = 1, \cdots, Q-1)$

Assumption 2: If $\theta_1 \le \theta_2 \le \cdots \le \theta_Q$ then $\cos\theta_Q - \cos\theta_1 \ge \frac{\lambda}{d}\left(\frac{2}{M} - 1\right)$

Proof: The function inside the bracket of equation (3-13), i.e. $\left|F_q(k)\right|^2$ in equation (A-2), is maximum at:

$$k_q = -\frac{Kd}{\lambda}\cos(\theta_q) \qquad for \qquad q = 1, 2, \cdots, Q \tag{3-15}$$

and its main-lobe is between:

$$k_q - \frac{K}{M} \le k \le k_q + \frac{K}{M} \qquad for \quad q = 1, 2, \cdots, Q \tag{3-16}$$

$\left|F_q(k)\right|^2$ is shown in Figure 3-1. The amplitude of the function is M^2 at the maximum point shown by A_1 in the figure.

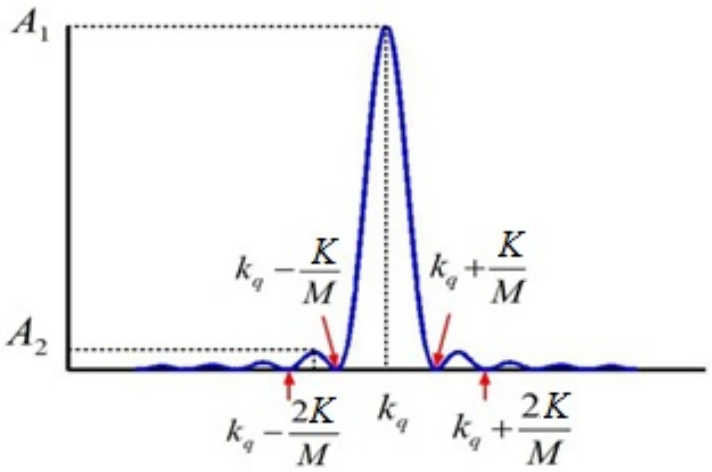

Figure 3-1. $\left|F_q(k)\right|^2$ *versus k*

In order to find the exact maximum and minimum points of $\left|F_q(k)\right|^2$, the following equation needs to be solved (if K goes to infinity Θ can be approximated as a continuous variable and derivative becomes applicable):

$$\frac{d}{d\Theta}\left(\frac{\sin M\Theta}{\sin\Theta}\right)^2 = 0 \tag{3-17}$$

where Θ is given by $\Theta = \frac{\pi d\cos(\theta_q)}{\lambda} + \frac{\pi k}{K}$. Taking the derivative, we get:

$$2\left(\frac{\sin M\Theta}{\sin\Theta}\right)\left(\frac{M\cos(M\Theta)\sin(\Theta) - \cos(\Theta)\sin(M\Theta)}{\sin^2(\Theta)}\right) = 0 \tag{3-18}$$

Using Euler's equation inside the second bracket, equation (3-18) can be easily expressed as:

$$\left(\frac{\sin M\Theta}{\sin\Theta}\right)\left(\frac{[M-1]\sin([M+1]\Theta) - [M+1]\sin([M-1]\Theta)}{\sin^2(\Theta)}\right) = 0 \tag{3-19}$$

Equation (3-19) means that either:

$$\sin(M\Theta) = 0 \tag{3-20}$$

or

$$[M-1]\sin([M+1]\Theta) - [M+1]\sin([M-1]\Theta) = 0 \tag{3-21}$$

The roots of equation (3-20) are the locations of maximum of main-lobe in Figure 3-1. The roots of equation (3-21) are the locations of maximum points within the side-lobes. Unfortunately, a closed-form solution for equation (3-21) is not available, but with a very good approximation we can assume the maximum point of the first side-lobe (which has considerably higher energy than the others) occurs at:

$$\Theta = \pm\frac{3\pi}{2M} \tag{3-22}$$

or Equivalently at:

$$k \approx k_q \pm \frac{3K}{2M} \tag{3-23}$$

Note that k in equation (3-23) is the middle point of the first side-lobe in Figure 3-1. The amplitude of the function at this point, shown by A_2 in Figure 3-1, is:

$$A_2 = \frac{1}{sin^2\left(\frac{3\pi}{2M}\right)} \tag{3-24}$$

Thus:

$$\gamma = \frac{A_1}{A_2} = M^2\, sin^2\left(\frac{3\pi}{2M}\right) \tag{3-25}$$

The ratio γ is plotted in Figure 3-2. When *M* is large, equation (3-25) can be approximated as:

$$\gamma = M^2\left(\frac{3\pi}{2M}\right)^2 \approx 22.20 \tag{3-26}$$

As can be seen from Figure 3-2, even for small *M* , A_1 is much larger than A_2 which implies that one can safely assume that the energy of the main-lobe is much higher than the side-lobes. In other words, generally the side-lobes energy can be neglected in equation (3-13).

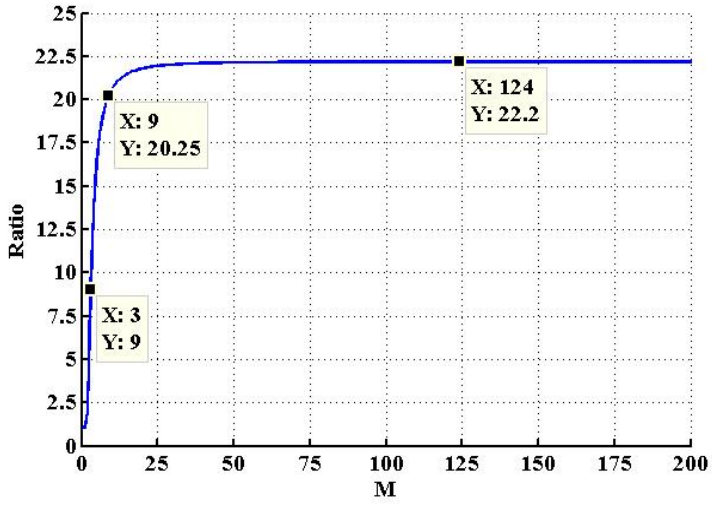

Figure 3-2. *The ratio of* A_1 *to* A_2

Equation (3-13) is the summation of positive functions. The maximum of each individual function, given by equation (3-15), is one of the Q largest peaks of the summation function in Equation (3-13) provided that its main-lobe is preserved. To this end, the following condition which is equivalent to Assumption 1 must be satisfied for every pair of adjacent DOAs (see Figure 3-3):

$$k_{i+1} - \frac{K}{M} \geq k_i + \frac{K}{M} \qquad for \quad i = 1, 2, \dots, Q-1 \tag{3-27}$$

$\left|F_q(k)\right|^2$ is periodic with *K*. If the main-lobe of k_1(corresponding to θ_1) approaches the left boundary ($k = -l\,, l$ is given in equation (3-3)), or k_Q (corresponding to θ_Q) approaches to the right boundary of spectrum ($k = l$), there is a chance of overlapping between the main-lobes of the first and last signal as shown in Figure 3-4. To avoid this case, the following condition must be satisfied (in the following equation if k_1 and k_Q are substitute with equation (3-15) we get Assumption 2):

$$k_1 - \frac{K}{M} + K \geq k_Q + \frac{K}{M} \tag{3-28}$$

■

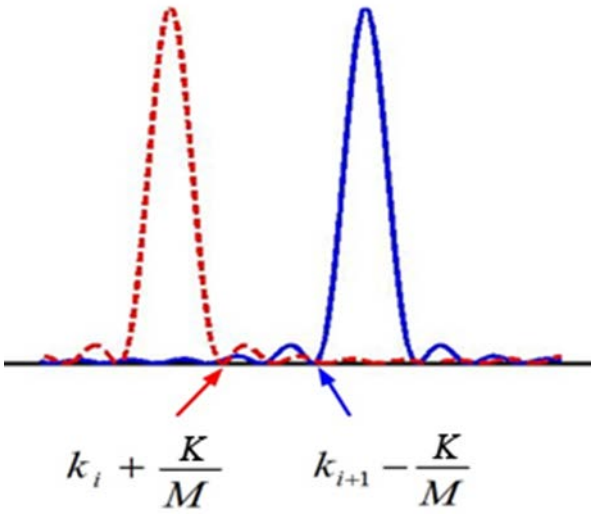

Figure 3-3. *To preserve the main-lobes, there must be no overlap between them*

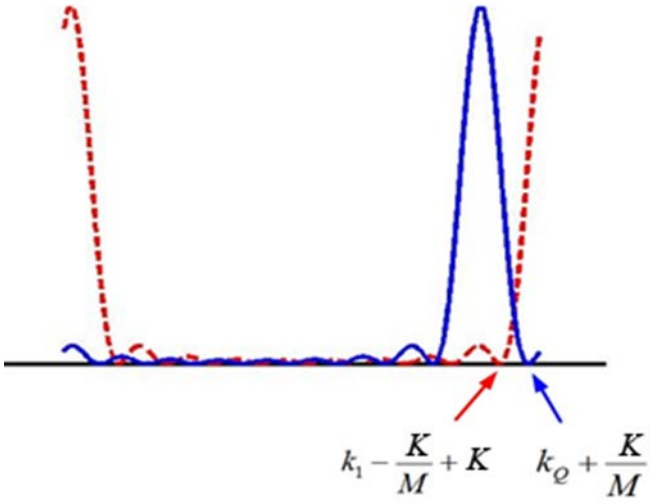

Figure 3-4. *Overlapping due to the periodicity*

3.4 Summary

In this chapter, first we reviewed the approach introduced in [53] and [13] which provides a DOA estimation technique for a noise-free environment when the number of sensors, *M*, goes to infinity and then provided a proof for that. In section 3.3, we introduced a new approach based on the spatial DFT which can estimate the DOA in a severely noisy environment with a low number of sensors. As it will be illustrated in the next chapter, the introduced approach is very fast and with just a small number of snapshots can determine the DOA. Also, it was shown that the energy of the main-lobe in DFT spectrum is much higher than the side-lobes and one can generally neglect the side-lobes. In addition, two assumptions were formulated to avoid overlapping in DFT spectrum.

Chapter 4

Performance Evaluation of the spatial DFT algorithm

4.1 Simulation

Extensive simulations were conducted and different features of the spatial DFT technique such as, accuracy, resolution, sensitivity to noise, effect of multiple snapshots and the number of sensors were evaluated and compared with those of existing techniques. The term *resolution of DOA estimation* is used to denote the minimum angle difference between two DOAs that can be resolved by the estimation technique.

In this regard, five different cases are presented. In example one, the basic performance and accuracy of the spatial DFT method will be evaluated. In Example 2, the effect of number of snapshots on the DOA estimation, using the spatial DFT technique and existing techniques will be compared. In example 3, the resolution of DOA estimation for different algorithms will be assessed. In Example 4, the effects of noise on the estimation accuracy for different algorithms will be investigated. Example 5 deals with inter-element spacing of the arrays' elements and finally in example 6 the effect of the number of sensors that make up the array is analyzed. In all simulations $K = 10000$ point DFT is considered and applied to obtain spatial DFT spectrum.

Example 1.

Consider an *M*-element uniform linear array with half-wavelength space between elements ($d = \lambda/2$) in a noise-free environment. Seven users with DOAs equal to

$[27^o, 50^o, 75^o, 98^o, 120^o, 142^o, 165^o]$ are present. To evaluate the accuracy of estimated DOA, RMSD (root-mean-square deviation) is measured as follows:

$$RMSD = \sqrt{\frac{\sum_{q=1}^{Q}(\theta_q - \hat{\theta}_q)^2}{Q}} \tag{4-1}$$

where θ_q and $\hat{\theta}_q$ are the actual and estimated DOA respectively. In this simulation transmitted data is randomly generated with normal distribution. Figure 4-1 shows $|\mathbf{X}_n(k)|^2$ using only one snapshot for the case when *M*=50. (in example 4 we will see how the performance of algorithm changes when the number of sensors varies). Clearly, the delta function approximation considered in equation (3-8) is justified.

From Figure 4-1 and equation (3-6) the estimated DOAs are:

$Estimated\ DOAs$: [27.0008 49.9841 74.9774 98.0247 119.9868 141.9990 165.0164]

which is very close to real DOAs and give accuracy of *RMSD=0.094* degrees.

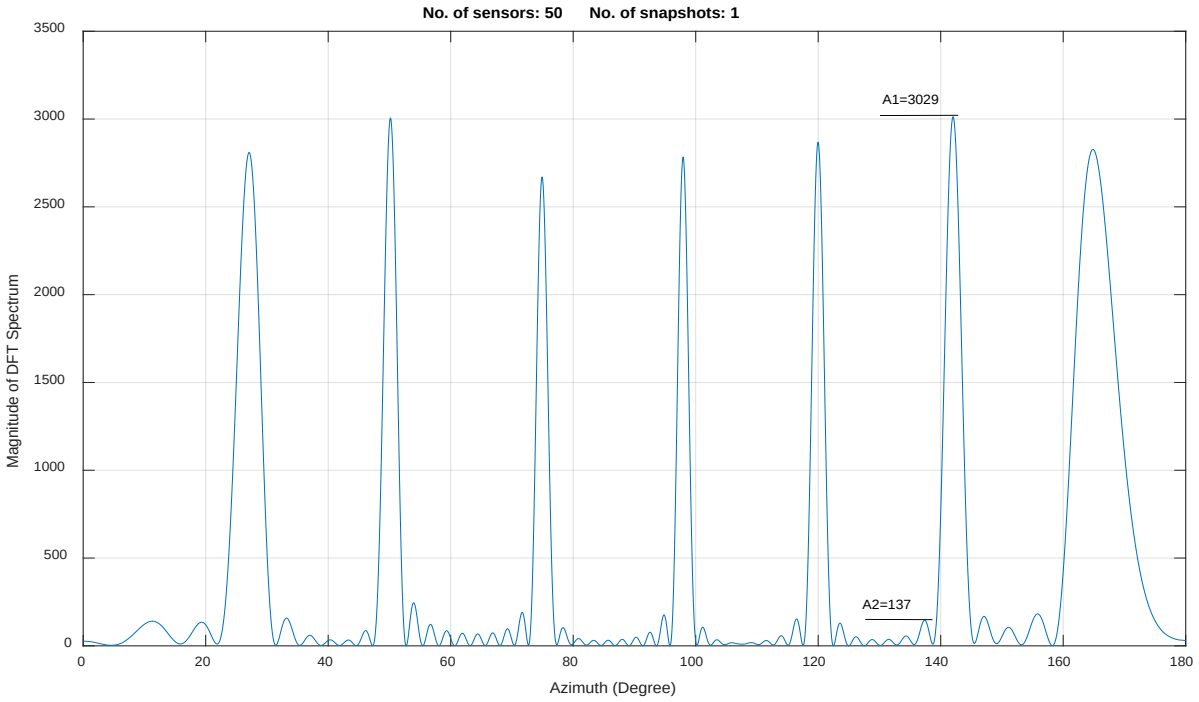

Figure 4-1. $\left|\mathbf{X}_n(k)\right|^2$ *for one snapshot when M=50*

Further, it can be seen that the ratio of the amplitude of the main-lobe versus the first side-lobe for one of the peaks, as shown in Figure 4-1, is equal to $\gamma = \frac{A_1}{A_2} = \frac{3029}{137} = 22.1$ which is consistent with proposition 3 and indicates that in general, even with limited number of sensors one can safely neglect the side-lobe energy.

Example 2.

In this experiment the performance of the proposed method is compared with existing methods in terms of number of snapshots. A 20-element ULA is used with an inter-element spacing of λ/2, where λ is the wavelength of the incident radiation. The source scenario consisted of five sources

located at $\theta = [\ 27°\quad 50°\quad 98°\quad 130°\quad 165°\ ]$. Gaussian white noise with a signal to noise ratio (SNR) = 20 dB is also added.

The number of snapshots was set to two different values: 1 and 10. The relative performance of Bartlett algorithm, MUSIC and spatial DFT method is investigated.

Figure 4-2, Figure 4-3 and Figure 4-4 shows the DOA estimation using Bartlett, MUSIC and spatial DFT method respectively for 1 and 10 snapshots. As can be seen, Bartlett and MUSIC algorithms failed to detect all sources with one snapshot. DOA estimation obtained from Bartlett is $\hat{\theta} = [46°\quad 98°\quad 166°]$ and the two other directions are missed. As can be seen from Figure 4-3, MUSIC algorithm is completely unable to estimate DOA with one snapshot. When the number of snapshots is increased to 10, with the other conditions remaining unchanged, the MUSIC and Bartlett algorithms can accurately estimate the DOA of incident signals. The proposed spatial DFT method, on the other hand, can accurately estimate DOA of all signals with just one snapshot. This indicates that one advantage of the spatial DFT algorithm is speed of response, i.e., it can accurately estimate the DOA with fewer snapshots than other algorithms.

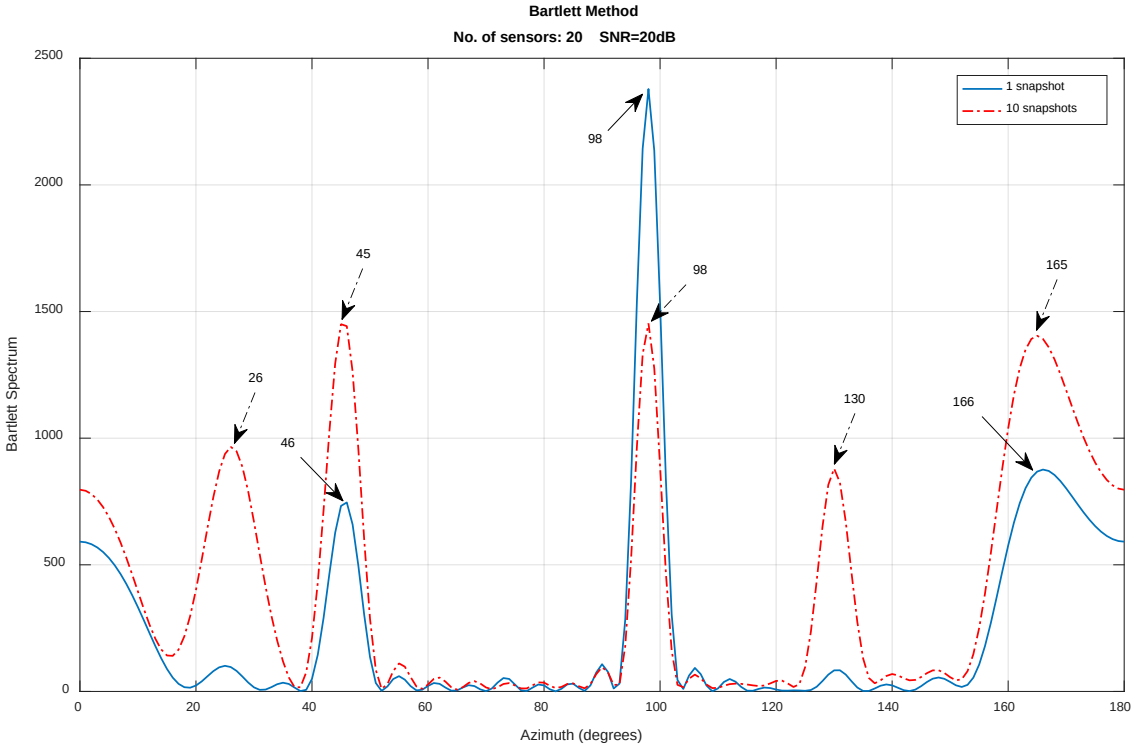

Figure 4-2. *Effect of number of snapshots on Bartlett method*

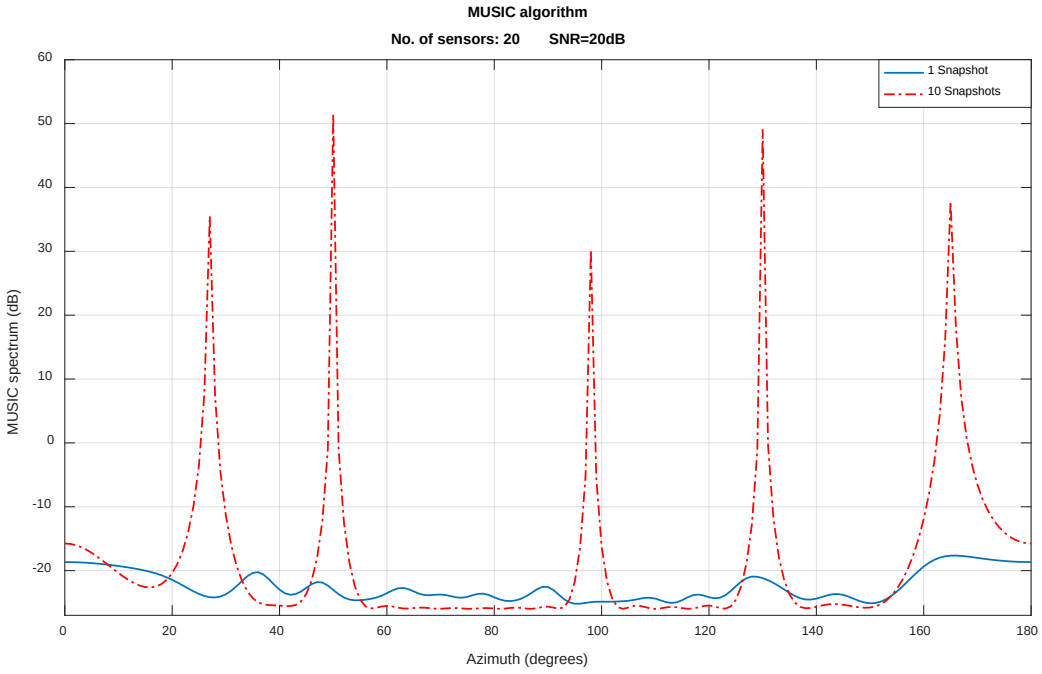

Figure 4-3. *Effect of number of snapshots on MUSIC algorithm*

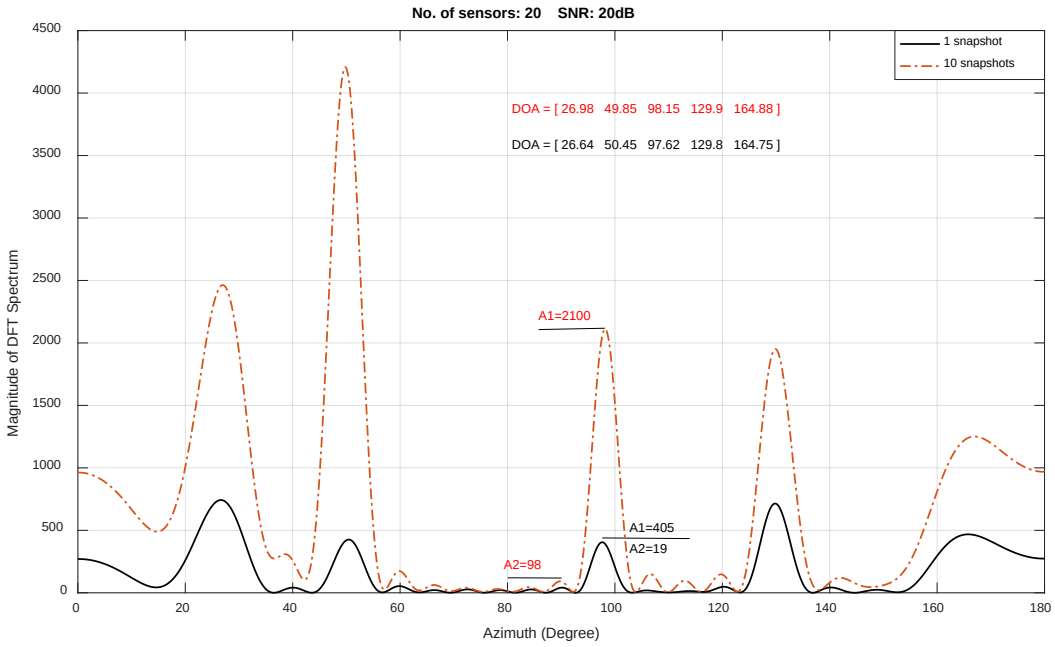

Figure 4-4. *Effect of number of snapshots on Spatial DFT*

The amplitudes of the main-lobe and the first side-lobe for one of the peaks are also shown in Figure 4-4. As can be seen their ratio γ in the case of one snapshot is equal to $\frac{A_1}{A_2} = \frac{405}{19} = 21.3$ and in the case of 10 snapshots the ratio γ is $\frac{A_1}{A_2} = \frac{2100}{98} = 21.42$. As it is expected from equation (3-26), the number of snapshots does not affect the ratio γ . In both cases the energy of the main-lobe is much higher than that of the side-lobes.

Example 3.

This simulation deals with a case where the DOAs of four signals are closely distributed. Again, a ULA with a spacing of λ/2 deployed at the receiver was considered. It was assumed that the DOAs of the target signal components were at $\theta = [45° \quad 47° \quad 134° \quad 136°]$. The performance

of the proposed method will be compared with Bartlett and MUSIC for the case of 160 sensors, 5 snapshots and SNR equal to 20 dB.

Figure 4-5 shows the result of Bartlett method. As can be seen even with 160 elements in the array and 5 snapshots, Bartlett cannot distinguish between angles 45˚ and 47˚ nor between angles 134˚ and 136˚. Figure 4-6 shows the result of MUSIC algorithm. As can be seen MUSIC algorithm is unable to determine the DOA of 4 closely spaced sources with angular separation of 2˚. Spatial DFT method, however, can determine all four sources with good accuracy as it is evident from the results in Figure 4-7.

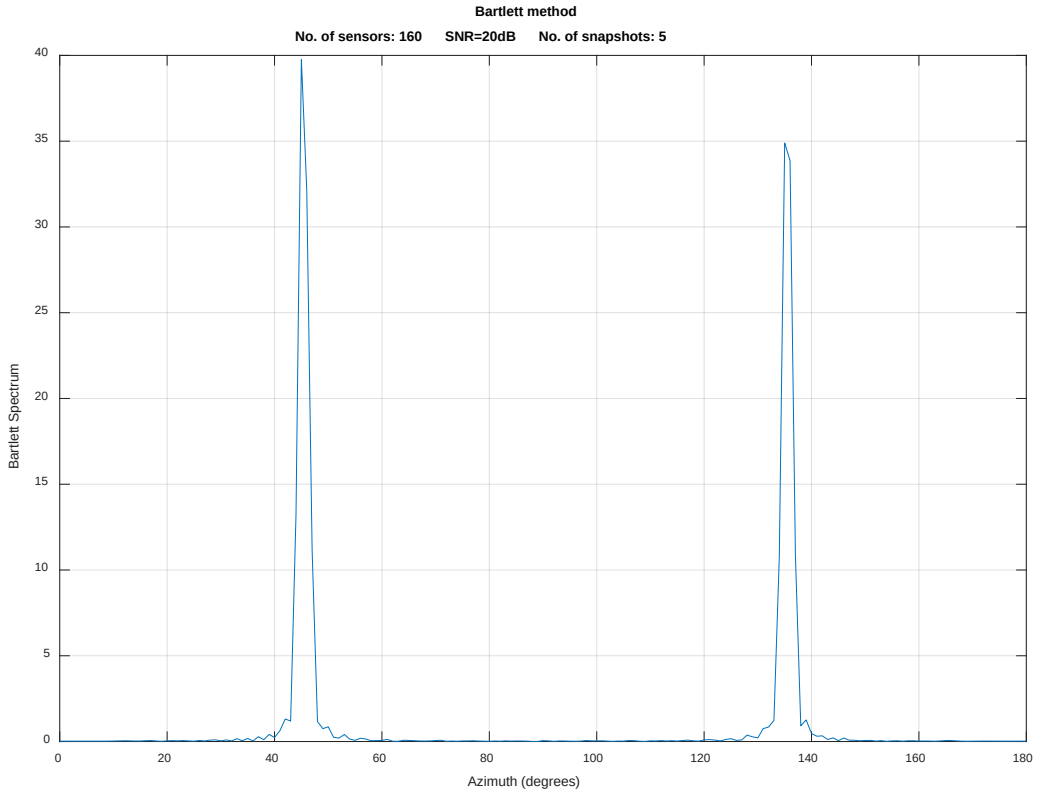

Figure 4-5. *Resolution of Bartlett method*

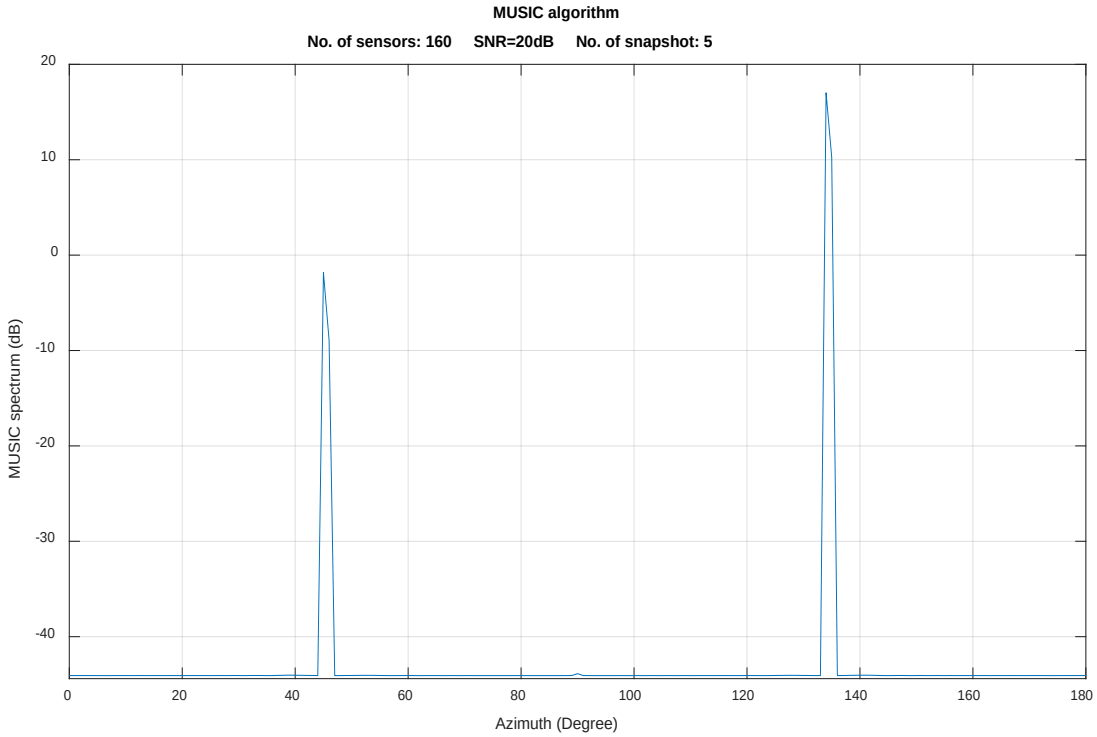

Figure 4-6. *Resolution of MUSIC algorithm*

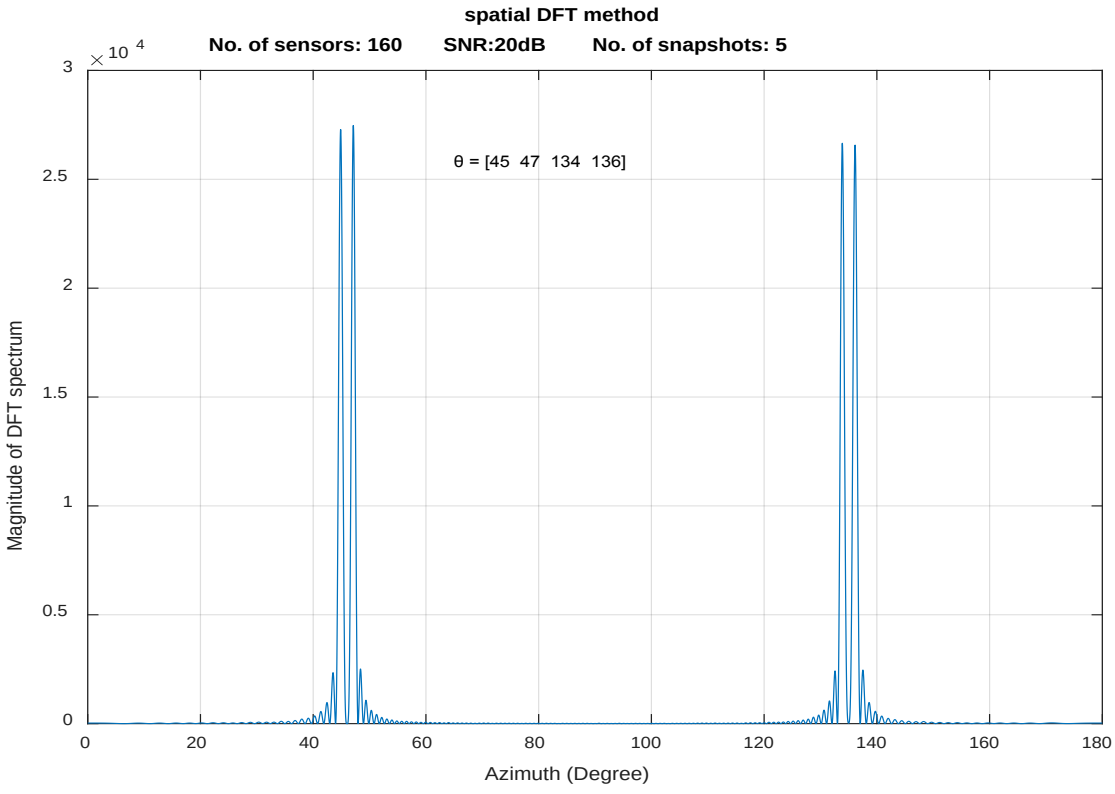

Figure 4-7. *Resolution of Spatial DFT method*

Simulations have shown that the DFT method is capable to estimate angular separation of 1° even for a smaller number of sensors and 5 snapshots. Since assumption 1 is not satisfied in the case of 1° separation, some overlapping will happen between the main-lobes of two adjacent signals. The overlapping, however, is not severe and still two main lobes are clearly distinguishable. Figure 4-8 shows the result of DFT method for the case of 1°separation when $\theta = [45° \quad 46° \quad 135° \quad 136°]$ with 120 sensors.

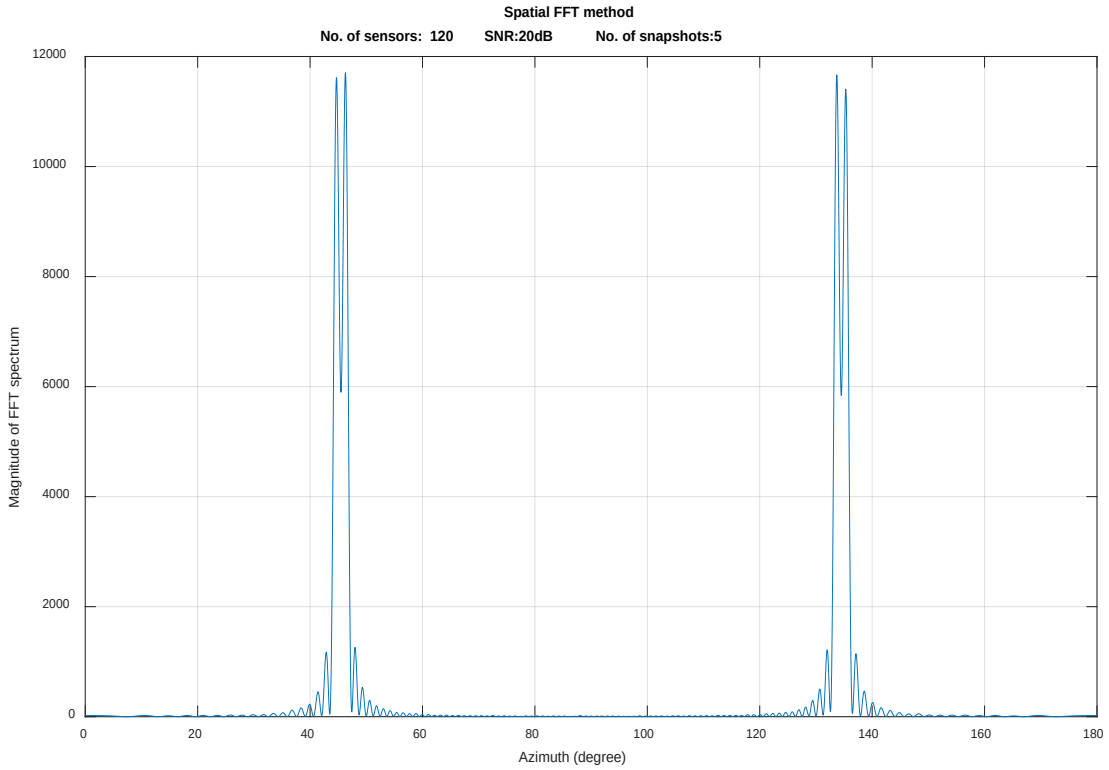

Figure 4-8 *Resolution of Spatial DFT method in angular separation of 1 degree*

Example 4.

In example four, effort has been made to study the effect of noise on the performance of different DOA algorithms since background noise is an important factor for practical implementation.

There are five narrow band signal sources with the same incident angles as in example two. Signals are not correlated, the noise is ideal Gaussian white noise, the element spacing is half of the input signal wavelength, the number of array elements is 20, the number of snapshots is 20, and the SNR is either 0 dB or 20 dB.

As can be seen from Figure 4-9 the SNR severely affects the performance of the Bartlett method and it deteriorates sharply with decreased SNR. For low SNR, there is no clear difference between the noise level and the peak of the Bartlett spectrum, leading to fake DOAs or errors in DOA estimation. Also, the estimated DOA has some error.

The MUSIC algorithm also has weak performance in the presence of low SNR. Results are shown in Figure 4-10. As expected, with an increase in the SNR, the performance of Bartlett and MUSIC are improving. The dashed lines in Figure 4-9 and Figure 4-10 shows the estimated DOA when the SNR=20 dB.

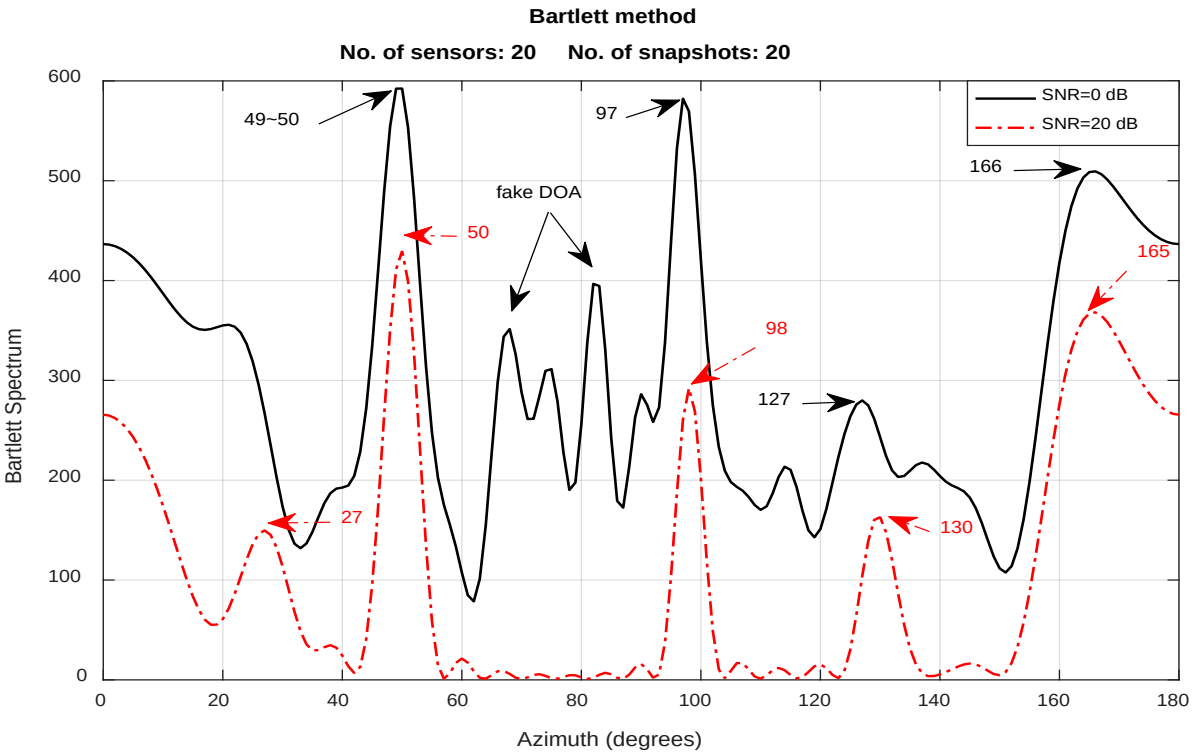

Figure 4-9. *Effect of noise on Bartlett method*

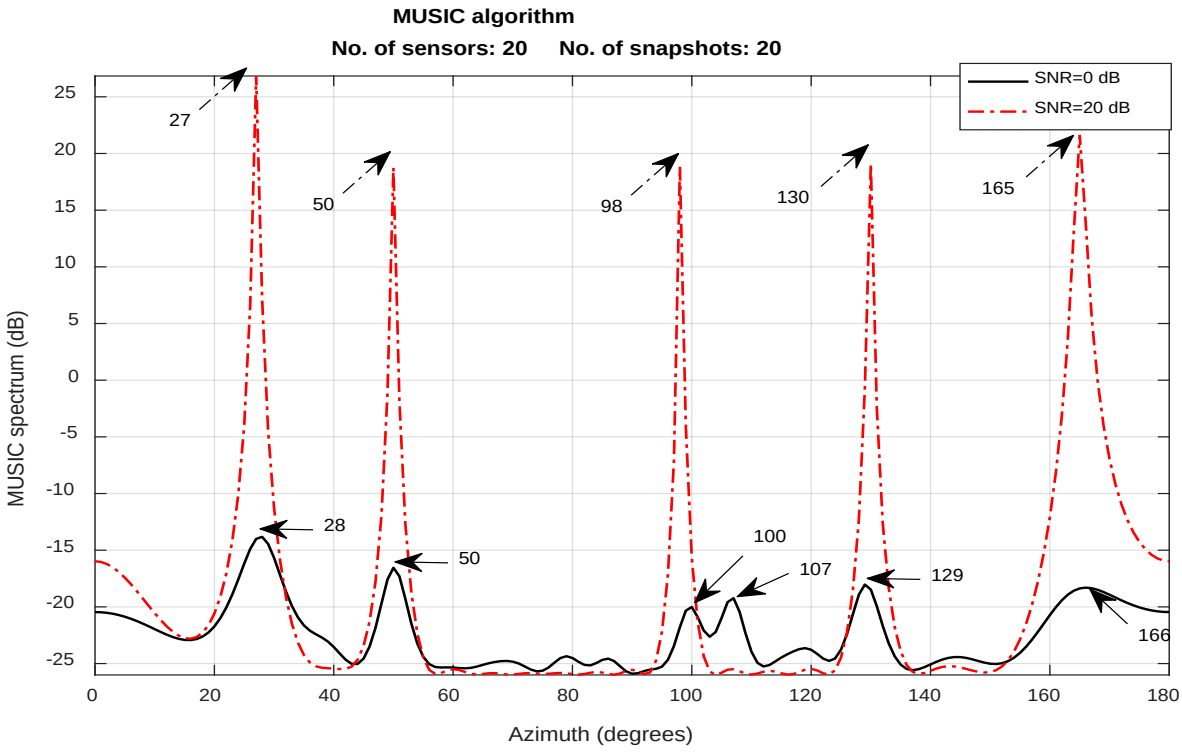

Figure 4-10. *Effect of noise on MUSIC algorithm*

On the other hand, the proposed spatial DFT method is very robust to noise. From Figure 4-11 it is clear that the spatial DFT method can accurately estimate the DOA in a severely noisy environment. For this algorithm, another experiment with severe noise (SNR = -5 dB) has been added. As it is expected from equation (3-12) and shown in Figure 4-11, the noise effect is approximately constant over the DFT spectrum. This indicates that the Spatial DFT method has superior robustness to noise when compared to existing techniques.

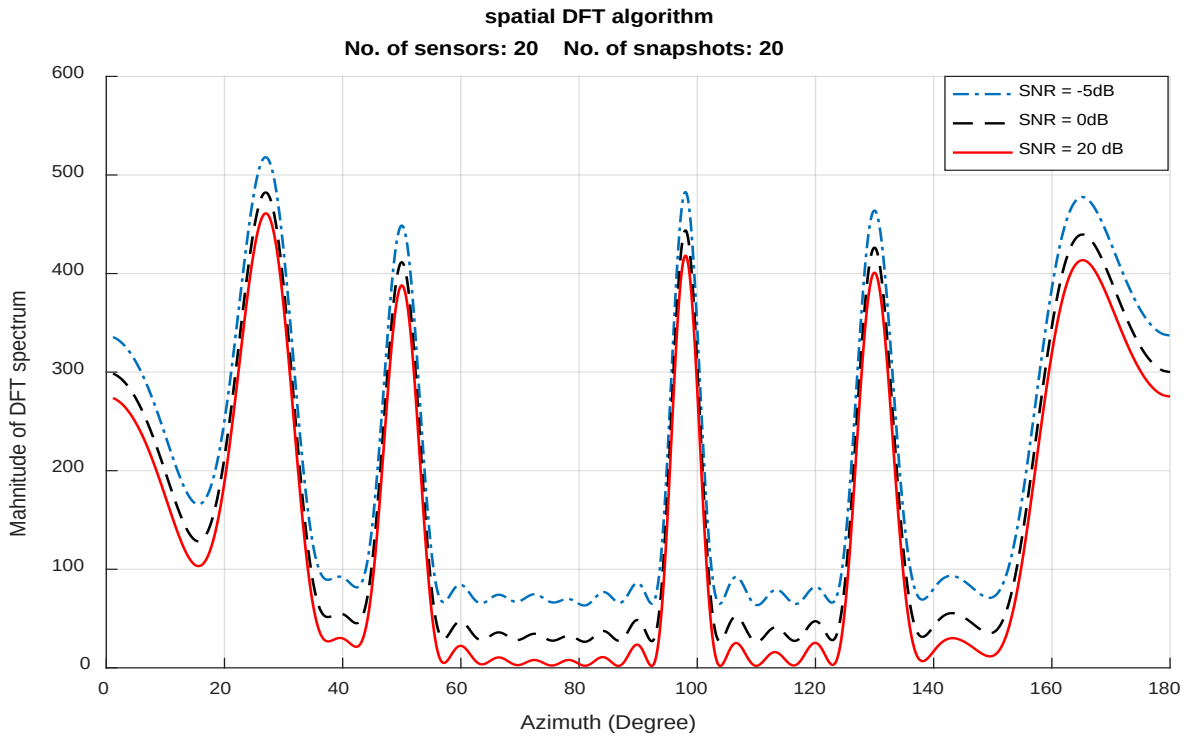

Figure 4-11. *Effect of noise on spatial DFT algorithm*

To illustrate how SNR and number of snapshots affect the performance for these three methods, Figure 4-12 shows the trend of RMSD error in DOA estimation in terms of SNR changes for 3 snapshots, 10 snapshots, 20 snapshots and 40 snapshots. As it can be seen, the spatial DFT method has the least RMSD error and the Bartlett method has the largest RMSD error. Also, with an

increased number of snapshots, the RMSD error will decrease in all methods. These results indicate that the proposed method has better performance than existing techniques in a noisy environment when only few snapshots are available.

Also, as can be seen, MUSIC algorithm is more sensitive to number of snapshots when compared to Bartlett and spatial DFT.

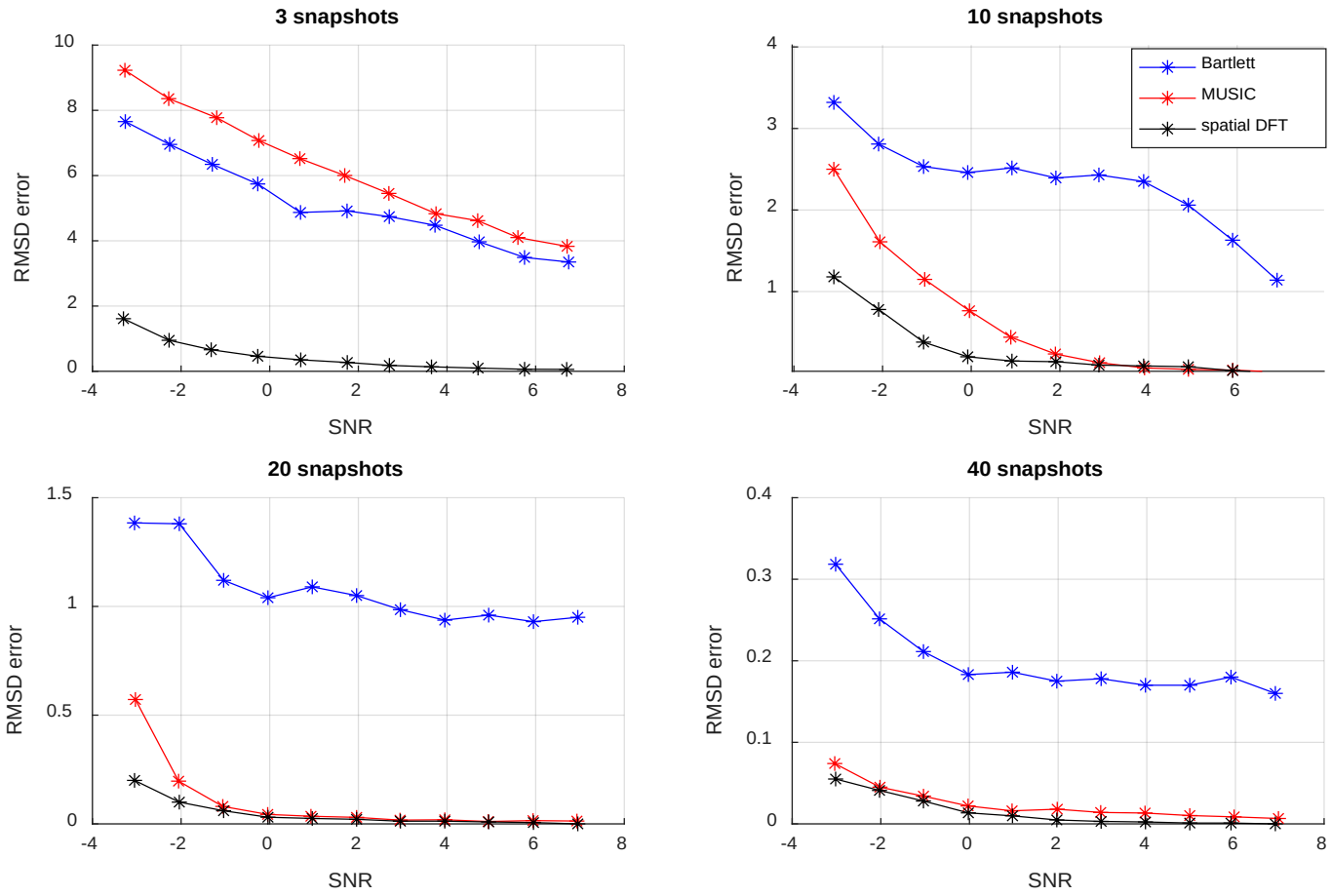

Figure 4-12. *Effect of noise and multi-snapshot on three methods*

Example 5

In this example we explore the effect of inter-element spacing and number of sensors on different methods. A 20-element ULA deployed at the receiver was considered and three signals with

incidence angles of $[30°\quad 70°\quad 140°]$ impinging on the array in the presence of noise with SNR=20 dB. Figure 4-13 shows the spectra for the three methods. Blue, red and black lines show the spectrum when inter-element spacing is equal to 0.25λ, 0.5λ and 0.75λ respectively. As can be seen if array spacing is greater than λ/2, then aliasing will happen, and some fake peaks occur in the spectrum of Bartlett and MUSIC and, if the array spacing is less than λ/2, the beam-width of peaks are wider. In [55] a method is proposed that can provide for the exact specification of the beam width and improve the directivity of compact arrays with inter-element spacing smaller than λ/2. It is important to note that superdirective arrays (having an element spacing less than λ/2) can have very poor efficiency and sensitivity properties if the amplitude of the invisible lobes is not controlled.

Regarding the spatial DFT method, if we check the validity for assumption 2, we end up with $cos\,\theta_Q - cos\,\theta_1 = (-1.62) \geq \frac{\lambda}{d}\left(\frac{2}{M} - 1\right) = -0.9(\frac{\lambda}{d})$.

Assumption 2 is satisfied for d=0.25λ and d=0.5λ but not for d=0.75λ. As long as assumptions 1 and 2 are satisfied we can get correct DOA estimation using equation (3-6). Blue and red graphs of the DFT spectrum, corresponding to d=0.25λ and d=0.5λ, indicate DOA of $[30°\quad 70°\quad 140°]$ degrees while the black graph which corresponds to d=0.75λ indicates DOA of $[55°\quad 70°\quad 118°]$ which is not the correct DOA estimation.

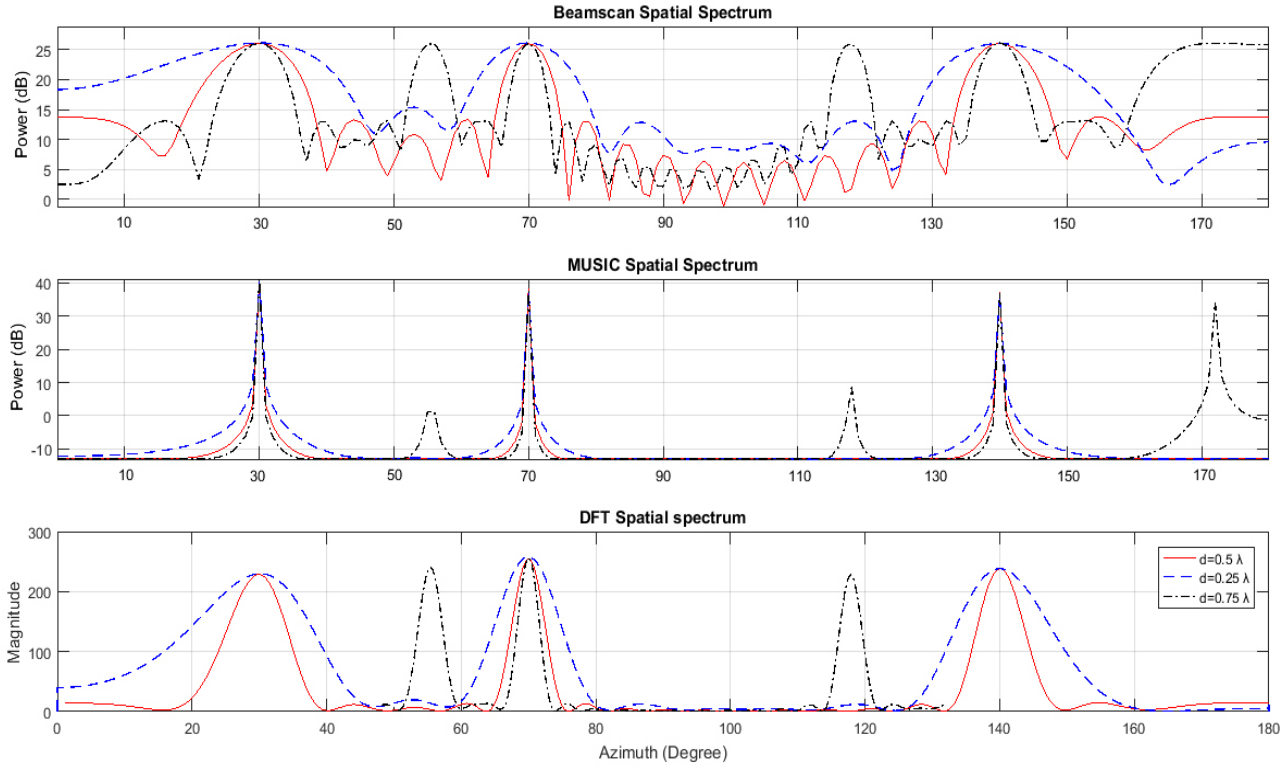

Figure 4-13. *Effect of element spacing. M=20*

Example 6

Now we illustrate the effect of the number of sensors elements on the performance of different DOA algorithms. Suppose that five sources located at $\theta = [\ 35°\quad 65°\quad 98°\quad 130°\quad 155°\ ]$ are impinging on an ULA with an inter-element spacing of λ/2. The signal to noise ratio (SNR) =20 dB. The number of snapshots was set to 10. Figure 4-14 shows the spatial DFT spectrum for different numbers of sensors. Blue, red, black and green spectrums are related to 20, 15, 10 and 7 elements respectively. As shown in Figure 4-14, with a decreasing number of sensors, the beam-width will increase and with 7 sensors the spatial DFT method fails to determine all sources. Figure 4-15 illustrates the same performance for Bartlett algorithm. In Figure 4-16 the MUSIC spectrums for four different numbers of sensors are shown and as can be seen, with decreasing the number of

elements, the beam-width will increase. MUSIC algorithm, however, still can estimate DOA of all sources accurately. As a result, in the case of a small number of sensors, the MUSIC algorithm has better performance than other techniques. However, this superiority is achieved at high computation. The MUSIC algorithm is having the computational complexity of the order of M^3 [56]. Also, the algorithm needs to search for the Q largest peaks and this increases the computational complexity. This is larger than the cost of the Bartlett algorithm, which is of the order of M^2 [57] [58]. On the other hand, using FFT to compute DFT of array output, the spatial DFT method has computational complexity of $O(M \log M)$ [59]. Figure 4-17 shows the required time for three methods to estimate the DOAs of the five sources in terms of different number of sensors.

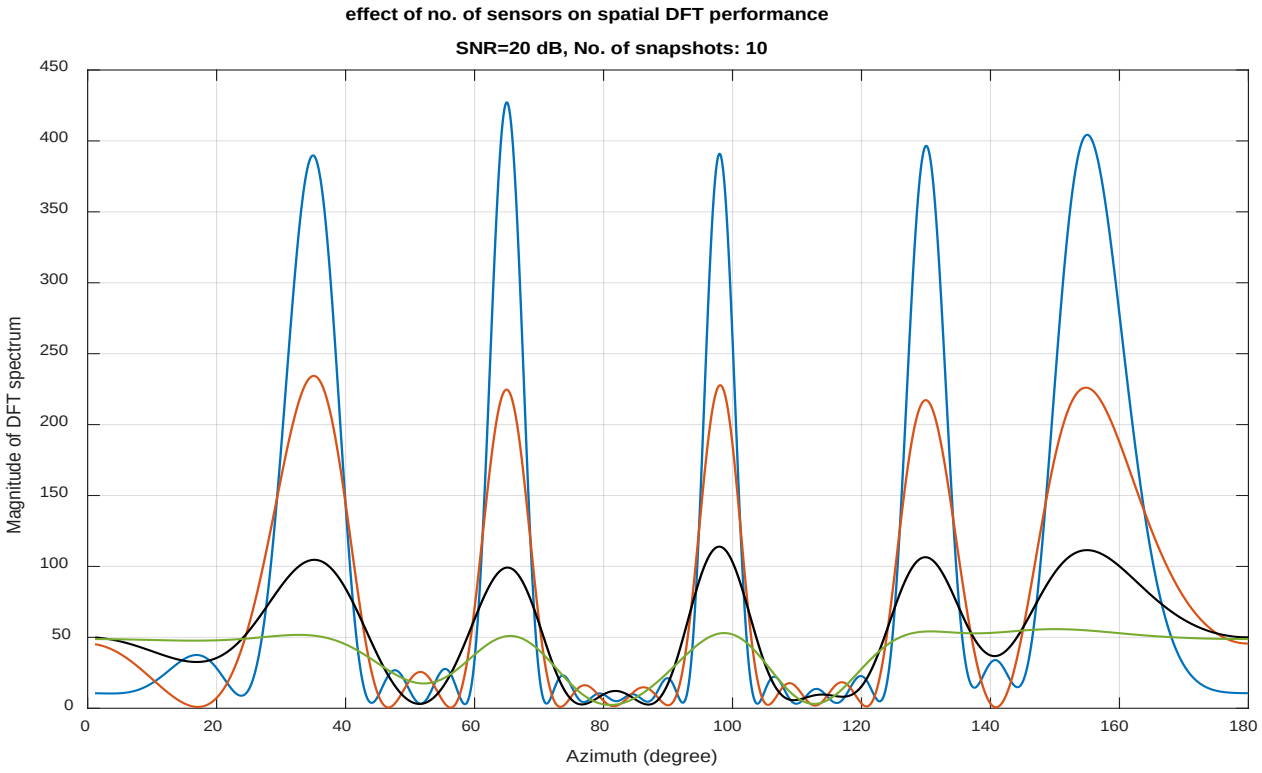

Figure 4-14. *Effect of no. of sensors on spatial DFT performance*

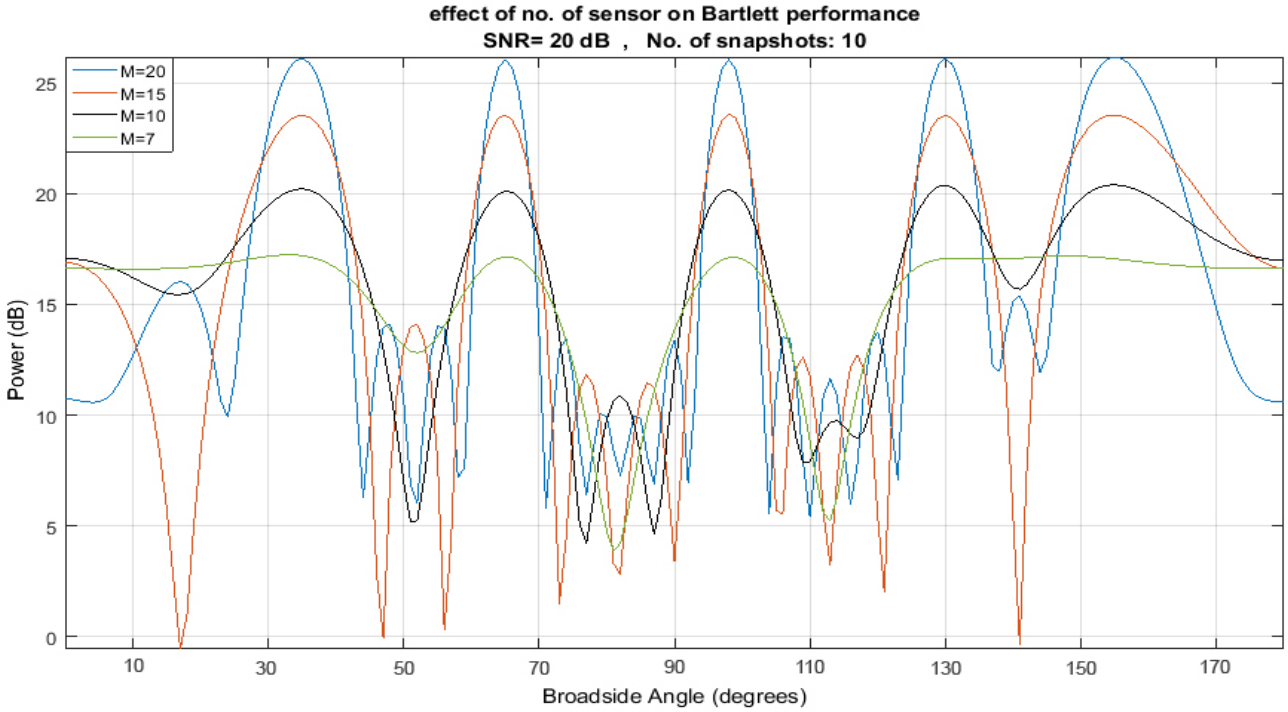

Figure 4-15. *Effect of no. of sensors on Bartlett performance*

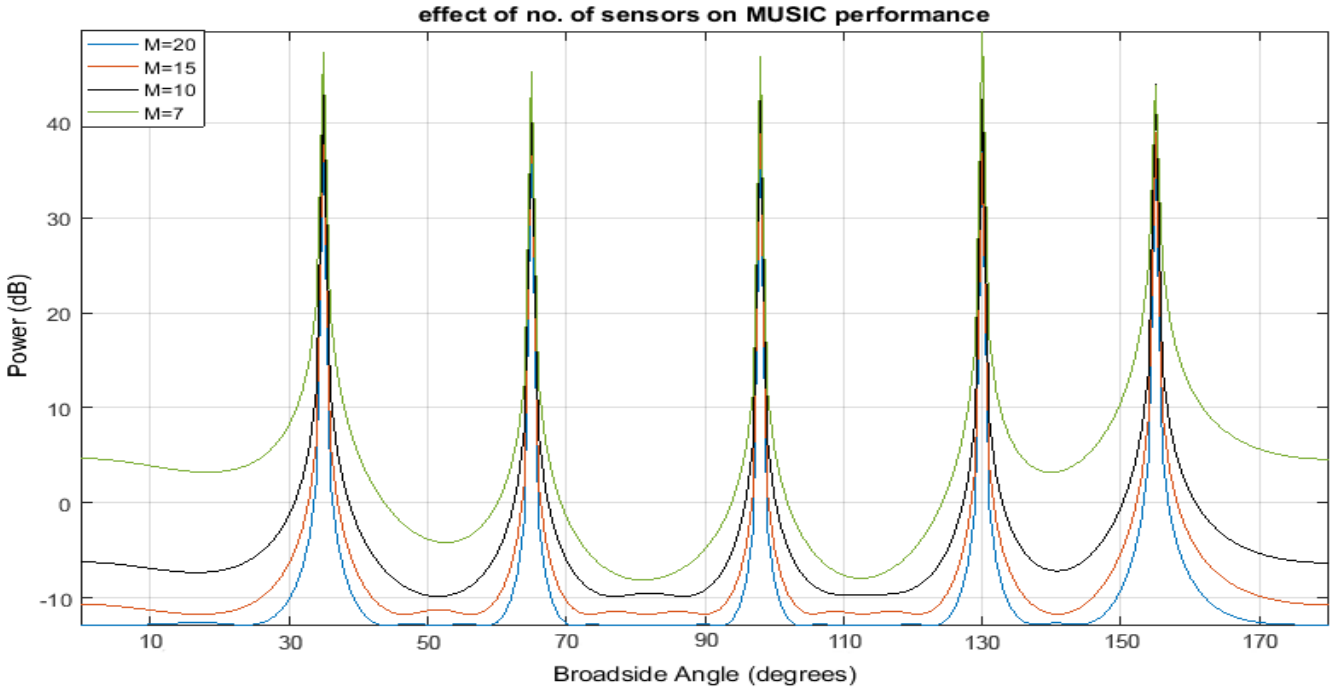

Figure 4-16. *Effect of no. of sensors on MUSIC performance*

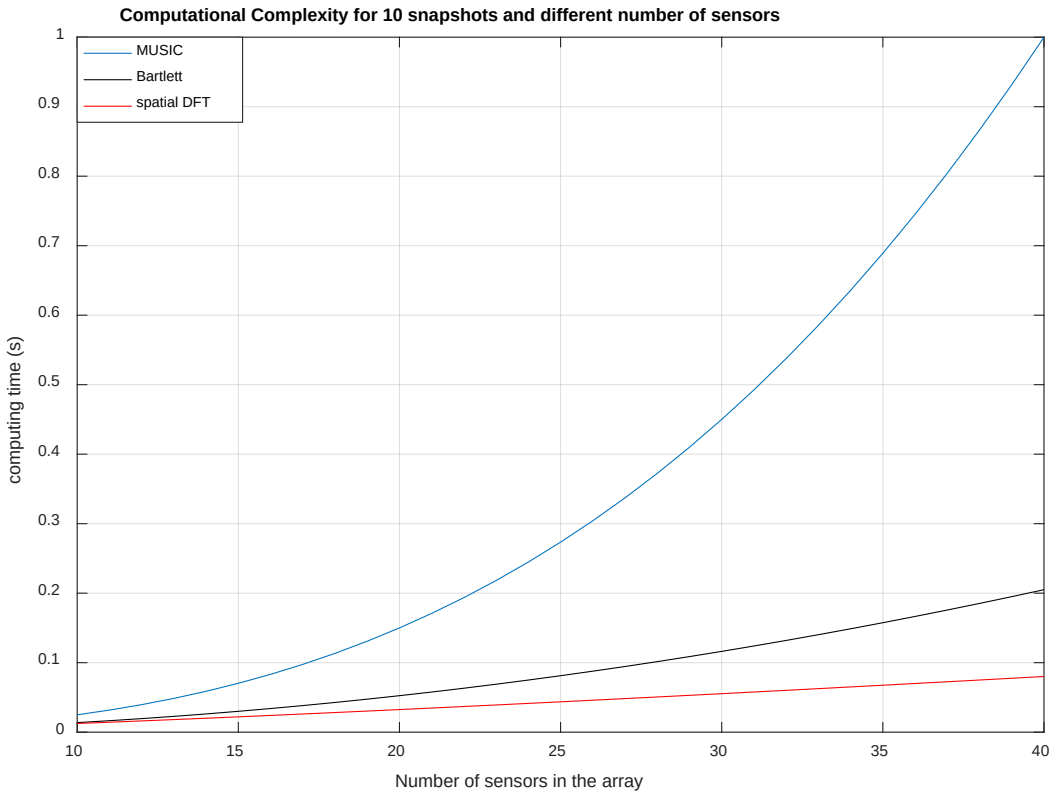

Figure 4-17. *Elapsed time for estimating DOAs by three methods*

4.2 Summary

In this chapter, 5 experiments have been simulated to evaluate the performance of the spatial DFT method and compare its performance with other techniques. The presented simulations show that the proposed spatial Discrete Fourier Transform algorithm, in most aspects such as fast responding, resolution and robustness to noise, has a better performance when compared to the conventional beamformer and MUSIC. However, regarding the required number of sensors to accurately estimate all DOAs, MUSIC outperforms the spatial DFT algorithm for small numbers of sensors.

Chapter 5

Conclusion and Future Work

5.1 Conclusion

This thesis dealt with the proposed spatial DFT method for DOA estimation. In chapter 2 the most commonly used DOA estimation techniques, such as the conventional beamformer, Minimum Variance Distortion-less Response (MVDR), maximum likelihood (ML), Multiple Signal Classification (MUSIC) and Estimation of Signal Parameters via Rotational Invariance Technique (ESPRIT) were reviewed and advantages and drawbacks for each method were outlined.

In chapter 3, an efficient DOA estimation algorithm, as modified spatial DFT, was proposed to evaluate and improve the DOA estimation algorithm introduced in [13]. In [13], which is based on the Fast Fourier Transform of the sensor array output data, a relationship between the FFT spectrum and the direction of arrival angles is established. According to [13], if the number of sensors M is sufficiently large and noise is negligible, the locations of the Q largest peaks of $|\boldsymbol{X}_n(k)|$ given by equation (3-6) can provide an asymptotically-consistent estimate of DOAs.

In chapter 3, propositions 2 and 3, it was shown that, if at least one of the conditions (M is large and noise is negligible) is not true, an average of $|\boldsymbol{X}_n(k)|$ over N_s snapshots can provide an asymptotically-consistent estimate of DOAs provided that N_s is sufficiently large and assumptions 1 and 2 of proposition 3 are satisfied.

In practice, in order to estimate the average of $\left|\boldsymbol{X}_{(n)}(k)\right|^2$, a *K*-point DFT needs to be applied to N_s subsequent snapshots ($n=1,2,...,N_s$). With N_s sufficiently large, the average over N_s approaches $E\left\{\left|\boldsymbol{X}_{(n)}(k)\right|^2\right\}$. In proposition 2, it was proved that the expected value of the output DFT over N_s snapshots can provide accurate DOA estimation even in the presence of noise.

In proposition 3 it was shown that the expected value of the DFT of the sensor array output provides accurate DOA estimation. In addition, we proved that even with small number of sensors, the maximum amplitude of the main-lobe in spatial DFT spectrum is much larger than maximum point of the first side-lobes (which has considerably higher energy than the other side-lobes). As a result, one can safely assume that the energy of the main-lobe is much higher than the side-lobes. In other words, the side-lobes energy can generally be neglected.

In chapter 4, an extensive simulation was conducted and different features of the spatial DFT technique such as, accuracy, resolution, sensitivity to noise, effect of multiple snapshots and the number of sensors were evaluated and compared with those of existing techniques. The results of simulations showed that the proposed algorithm is superior to MUSIC and Bartlett techniques with respect to resolution, required number of snapshots, dealing with noise and speed. It also has good performance when the number of sensors is comparatively small

5.2 Future work

In this thesis we used the Fourier transform as the main tool to estimate DOA. However, besides the Fourier transform, there are many other transforms that have been developed for signal analysis and can be used instead of the Fourier transform. Some of these transforms might have advantages

over the Fourier transform. For example, the computational complexity and storage cost of the spatial DFT algorithm, proposed in chapter 3, can be further reduced by employing Discrete Cosine Transfer (DCT).

Notice that the DCT basis vectors are real vectors, varying in a sinusoidal pattern with increasing frequency [60] [61] [62]. As a result, when using DFT, one must keep complex numbers and perform complex computations. In contrast, by using the DCT, one deals with real numbers, performing the computation with real numbers and storing real coefficients. Therefore, less memory is required and the computational cost decreases.

Furthermore, it is useful to examine and evaluate the performance of the proposed algorithm to sensor gain and phase perturbations. We expect the proposed algorithm to be more robust to these perturbations because it needs only a small number of snapshots, while the traditional DOA methods often involve taking a certain number of snapshots and are more subject to the effects of the sensor gain and phase perturbations occurring over the period of collecting snapshots. In addition, the sensitivity of the algorithm to the coefficients and element location can be explored.

The spatial DFT algorithm is based on narrow-band signals and we assume that received signals are narrowband. It would be worthwhile to investigate the possibility of extending the spatial DFT technique to wide-band signals.

Bibliography

[1] H. L. VanTrees, Detection, Estimation, and Modulation Theory, Optimum Array Processing, John Wiley & sons, 1968.

[2] S. Jeon, Y. Wang, Y. Qian and T. Itoh, "A Novel Smart Antennas System Implementation for Broad-Band Wireless Communications," *IEEE Trans. On Antennas and Propagation,* vol. 50, no. 5, pp. 600-606, May 2002.

[3] T. S. Rappaport, " Wireless personal communications: Trends and challenges," *IEEE Antennas and Propagation Magazine,* vol. 33, no. 5, pp. 19-29, Oct. 1991.

[4] Y. Huang and R. S. Wolff, "Mobile WiMAX Symposium, 2009. MWS '09. IEEE," in *Mobile WiMAX Symposium, IEEE*, Napa Valley, CA, USA, 2009.

[5] S. Bellofiore, "Smart Antenna System Analysis, Integration and Performance for Mobile Ad-Hoc Networks (MANETs)," *IEEE Trans. On Antennas and Propagation,* vol. 50, no. 5, pp. 571-581, May 2002.

[6] J. Capon, "High resolution frequency wavenumber spectrum analysis , Aug. 1969.," *Proceedings of the IEEE,,* vol. 57, no. 8, pp. 1408-1418, 1969.

[7] R. Schmidt, "A Signal Subspace Approach to Multiple Emitter Location," PhD Thesis, Stanford University, 1981.

[8] R. O. Schmidt, "Multiple Emitter Location and Signal Parameter Estimation," *IEEE TRANSACTIONS ON ANTENNAS AND PROPAGATION,* Vols. AP-34, no. 3, March 1986.

[9] A. Paulraj, R. Roy and T. Kailath, "A subspace rotation approach to signal parameter estimation," *Proceedings of the IEEE,* vol. 74, no. 7, pp. 1044-1046, 1986.

[10] R. Roy, A. Paulraj and T. Kailath, "ESPRIT-A subspace rotation approach to estimation of parameters of cisoids in noise," *IEEE Transactions on Acoustics, Speech, and Signal Processing,* vol. 34, no. 5, pp. 1340-1342, 1986.

[11] Z. Ke, M. Peng and Z. Jian-yun, "DOA Estimation Algorithm Based on FFT in Switch Antenna Array," in *2011 IEEE CIE International Conference on Radar*, 2011.

[12] J. Zhuang, H. Xiong, W. Wang and X. Cai, "FFT-based adaptive 2-D DOA estimation for arbitrary array structures," in *22nd International Conference on Digital Signal Processing (DSP)*, 2017.

[13] L. Tao and H. Kwan, "A novel approach to fast DOA estimation of multiple spatial narrowband signals," in *The 2002 45th Midwest Symposium on Circuits and Systems. MWSCAS-2002.*, Tulsa, OK, USA, 2002.

[14] A. J. Barabell, J. Capon, D. F. DeLong, J. R. Johnson and K. D. Senne, "Performance Comparison of Superresolution Array Processing Algorithms.," MASSACHUSETTS INST OF TECH LEXINGTON LINCOLN LAB, 1998.

[15] R. Roy and T. Kailath, "Estimation of signal parameters via rotational invariance techniques - ESPRIT," *IEEE Transactions on Acoustics, Speech, and Signal Processing,* vol. 37, no. 7, pp. 984-995, Jul. 1989.

[16] F. Gross, Smart Antennas for Wireless Communications, McGraw-Hill Education, 2005.

[17] B. A. Constantine and L. Panayiotis, Introduction to Smart Antenna, Morgan & Claypool Publishers, 2007.

[18] J. Choi, "Pilot channel-aided techniques to compute the beamforming vector for CDMA systems with antenna array," *IEEE Trans. Veh. Technol.,* vol. 49, pp. 1760-1775, 2000.

[19] S. Lim, J. Lee and J. Park, "Performance evaluation of adaptive beamforming using pilot and traffic channel in CDMA2000 reverse link," *IEEE Veh. Technol. Conf.,* vol. 4, pp. 2154-2157, 2002.

[20] N. Wang, P. Agathoklis and A. Antoniou, "A New DOA Estimation Technique Based on Subarray Beamforming," *IEEE TRANSACTIONS ON SIGNAL PROCESSING,* vol. 54, no. 9, 2006.

[21] W. Featherstone, H. Strangeways, M. Zatman and H. Mewes, "A novel method to improve the performance of Capon's minimum variance estimator," in *Tenth International Conference on Antennas and Propagation,*, 1997.

[22] P. Handel, P. Stoica and T. Soderstrom, "Capon method for doa estimation: accuracy and robustness aspects," in *IEEE Winter Workshop on Nonlinear Digital Signal Processing*, 1993.

[23] R. Lorenz and S. Boyd, "Robust Minimum Variance Beamforming," *IEEE TRANSACTIONS ON SIGNAL PROCESSING,* vol. 53, no. 5, 2005.

[24] S. Marpel, M. Adeli and L. Huaping, "Super-Fast algorithm for minimum variance (Capon) spectral estimation," in *Forty Fourth Asilomar Conference on Signals, Systems and Computers (ASILOMAR)*, 2010.

[25] R. Kumaresan and A. K. Shaw, "High resolution bearing estimation without eigendecomposition," in *Proc. IEEE Int. Conf. Acoust. Speech Signal Processing*, 1985.

[26] P. Stocia, "Maximum likelihood methods for direction-of-arrival estimation," *IEEE Transactions on Acoustics, Speech, and Signal Processing ,* vol. 38, no. 7, pp. 1132-1143, 1990.

[27] F. Bohme, "Estimation of Source Parameters by Maximum Likelihood and Nonlinear Regression," in *Proc. ICASSP '84*, 1984.

[28] J. Li and R. Compton, "Maximum likelihood angle estimation for signals with known waveforms," *IEEE. Trans. Signal Process.,,* vol. 41, no. 9, pp. 2850-2862, 1993.

[29] Z. Chen, G. Gokeda and Y. Yu, Introduction to Direction-of-Arrival Estimation, Artech House, 2010.

[30] Y. Bresler and A. Macovski, "Exact maximum likelihood parameter estimation of superimposed exponential signals in noise," *IEEE Trans. Acoust., Speech, Signal Process,* Vols. ASSP-34, no. 10, pp. 1081-1089, Oct 1986.

[31] P. Stoica and A. Nehorai, "Performance study of conditional and unconditional direction-of-arrival estimation," *IEEE Trans. Acoust., Speech, Signal Process.,* vol. 38, no. 10, pp. 1783-1795, Oct. 1990.

[32] I. Ziskind and M. Wax, "Maximum likelihood localization of multiple sources by alternative projection," *IEEE Trans. Acoust., Speech, Signal Process,* vol. 36, no. 10, pp. 1553-1560, 1988.

[33] J. Joshi and A. Dhande, "DIRECTION OF ARRIVAL ESTIMATION USING MUSIC ALGORITHM," *International Journal of Research in Engineering and Technology,* vol. 3, no. 3, pp. 633-636, 2014.

[34] H. Krim and M. Viberg, "Two decades of array signal processing research: The parametric approach," *IEEE Signal Process. Mag.,* vol. 13, no. 4, pp. 67-94, 1996.

[35] P. Gupta and S. Kar, "MUSIC and improved MUSIC algorithm to estimate direction of arrival," in *International Conference on Communications and Signal Processing (ICCSP)*, 2015.

[36] A. Kintz and I. Gupta, "A Modified MUSIC Algorithm for Direction of Arrival Estimation in the Presence of Antenna Array Manifold Mismatch," *IEEE Transactions on Antennas and Propagation,* vol. 64, no. 11, pp. 4836 - 4847, 2016.

[37] Q. Zhao and W. Liang, "A Modified MUSIC Algorithm Based on Eigen Space," *Advances in Intelligent and Soft Computing, Springer, Berlin, Heidelberg,* vol. 104, pp. 271-276, 2011.

[38] K. Kundu, "Modified MUSIC algorithm for estimating DOA of signals," *Signal Processing, ELSEVIER,* vol. 48, no. 1, pp. 85-90, 1996.

[39] A. J. Barabell, "Improving the resolution performance of eigenstructure-based direction-finding algorithms," *Proc. Int. Conf. Acoustics Speech, Signal Processing (ICASSP),* Vols. AP-34, pp. 336-339, 1983.

[40] C. T. Chiang and A. C. Chang, "DOA estimation in the asynchronous DS-CDMA system," *IEEE Trans. Antennas Propagation,* vol. 51, pp. 40-47, Jan. 2003.

[41] I. S. Reed, J. Mallett and L. Brennan, "Rapid convergence rate in adaptive arrays," *IEEE Transactions on Aerospace and Electronic Systems,* vol. 10, no. 6, pp. 853-863, Nov. 1974.

[42] R. Roy, A. Paulrajand and a. T. Kailath, "Direction-of-arrival estimation by subspace rotation methods—ESPRIT," *Proc. Int. Conf. Acoustics Speech, Signal Processing (ICASSP),* Vols. AP-34, pp. 2495-2498, April 1986.

[43] A. Molisch, Wireless communication, John Wiley and sons, Ltd., publication, 2011.

[44] H. Fang-Ming, "An ESPRIT-like algorithm for coherent DOA estimation," *IEEE Antennas and Wireless Propagation Letters ,* vol. 4, pp. 443-446, 2005.

[45] A. Gershman and F. Gao, "A generalized ESPRIT approach to direction-of-arrival estimation," *IEEE Signal Processing Letters,* vol. 12, no. 3, pp. 254-257, 2005.

[46] Y. Fayad, C. Wang and Q. Cao, "Improved ESPRIT method used for 2D-DOA estimation in tracking radars," in *European Radar Conference (EuRAD)*, 2016.

[47] W. Xudong, X. Zhang and J. Li, "Improved ESPRIT Method for Joint Direction-of-Arrival and Frequency Estimation Using Multiple-Delay Output," *International Journal of Antennas and Propagation,* vol. 2012, 2012.

[48] C. Mathews, "Improved closed-form DOA/frequency estimation via ESPRIT using DFT and derivative DFT beamforming," in *IEEE International Conference on Acoustics, Speech, and Signal Processing Conference Proceedings*, 1996.

[49] G. Xu, S. D. Silverstein, R. H. Roy and a. T. Kailath, "Beamspace ESPRIT," *IEEE. Trans. Signal Process,* vol. 42, no. 2, pp. 349-356, Feb. 1994.

[50] N. Tayem and H. M. Kwon, "Conjugate ESPRIT (C-SPRIT)," *IEEE Trans. Antennas Propag.,* vol. 52, pp. 2618-2624, Oct. 2004.

[51] Y. Hou, J. Huang and X. Feng, "The study on beam-space DOA estimator based on beamforming system," *Journal of Projectiles, Rockets, Missiles and Guidance,* vol. 27, no. 3, pp. 82-90, 2007.

[52] P. Stoica and A. Nehorai, "MUSIC, maximum likelihood and Cramer-Rao bound," *IEEE Trans. ASSP,* vol. 37, no. 5, pp. 720-741, 1989.

[53] I. Moazen and P. Agathoklis, "A Multistage Space–Time Equalizer for Blind Source separation," *Circuits, Systems, and Signal Processing,* vol. 35, no. 1, pp. 185-209, January 2015.

[54] I. Moazen, "internal technical report, personal communication," 2016.

[55] D. Shpak, "A method for the optimal pattern synthesis of linear arrays with prescribed nulls," *IEEE transaction on antennas and propagation,* vol. 44, no. 3, 1996.

[56] V. Madhava, S. Jagadeesha and T. Yerriswamy, "A COMPARATIVE STUDY OF DOA ESTIMATION ALGORITHMS WITH APPLICATION TO TRACKING USING KALMAN FILTER," *Signal & Image Processing : An International Journal (SIPIJ),* vol. 6, no. 6, 2015.

[57] C. Stockle, "DoA Estimation Performance and Computational Complexity of Subspace- and Compressed Sensing-based Methods," in *WSA 2015; 19th International ITG Workshop on Smart Antennas*, 2015.

[58] N. Anwar Baig and M. Bilal Malik, "Comparison of Direction of Arrival (DOA) Estimation Techniques for Closely Spaced Targets," *International Journal of Future Computer and Communication,,* vol. 2, no. 6, 2013.

[59] J. W. Cooley and J. W. Tukey, "An Algorithm for the Machine Calculation of Complex Fourier Series," *Mathematics of Computation,* vol. 19, no. 90, pp. 297-301, 1965.

[60] Y. Wang, J. Ostermann and Y. Zhang, Video Processing and Communication, Prentice Hall, 2002.

[61] N. Ahmed, T. Natarajan and K. R. Rao, "Discrete Cosine Transform," *IEEE Transactions on Computers,* Vols. C-23, no. 1, pp. 90-93, 1974.

[62] K. Rao and P. Yip, Discrete Cosine Transform: Algorithms, Advantages, Applications, Boston: Academic Press, 2014, 1990.

Appendix A
proof of Proposition 2

Proof: By replacing

$$t_q(n) = \left|t_q(n)\right| e^{j\angle t_q(n)} \tag{A-1}$$

$$F_q(k) = \frac{\sin\left(\frac{\pi d\,\cos(\theta_q)}{\lambda} + \frac{\pi k}{K}\right) M}{\sin\left(\frac{\pi d\,\cos(\theta_q)}{\lambda} + \frac{\pi k}{K}\right)}\, e^{-j\left(\left(\frac{2\pi}{\lambda}d\right)cos(\theta_q)+\frac{2\pi k}{K}\right)\left(\frac{M-1}{2}\right)} = \left|F_q(k)\right| e^{j\angle F_q(k)} \tag{A-2}$$

and

$$\boldsymbol{\Psi}_{(n)}(k) = \mathrm{Re}\left\{\boldsymbol{\Psi}_{(n)}(k)\right\} + j\ \mathrm{Im}\left\{\boldsymbol{\Psi}_{(n)}(k)\right\} \tag{A-3}$$

in equation (3-4), we get:

$$\boldsymbol{X}_{(n)}(k) = \sum_{q=1}^{Q} \left|t_q(n)\right|\left|F_q(k)\right| e^{j(\angle t_q(n)+\angle F_q(k))} + \mathrm{Re}\left\{\boldsymbol{\Psi}_{(n)}(k)\right\} + j\ \mathrm{Im}\left\{\boldsymbol{\Psi}_{(n)}(k)\right\} \tag{A-4}$$

$\left|\boldsymbol{X}_{(n)}(k)\right|^2$ can be expressed as:

$$\left|\boldsymbol{X}_{(n)}(k)\right|^2 = \left(\sum_{q=1}^{Q} \left|t_q(n)\right|\left|F_q(k)\right| \cos\left(\angle t_q(n) + \angle F_q(k)\right) + \mathrm{Re}\left\{\boldsymbol{\Psi}_{(n)}(k)\right\}\right)^2 + \left(\sum_{q=1}^{Q} \left|t_q(n)\right|\left|F_q(k)\right| \sin\left(\angle t_q(n) + \angle F_q(k)\right) + \mathrm{Im}\left\{\boldsymbol{\Psi}_{(n)}(k)\right\}\right)^2 \tag{A-5}$$

Equation (A-5) can be expanded as follows:

$$\left|\boldsymbol{X}_{(n)}(k)\right|^2 = \left(\sum_{q=1}^{Q} \left|t_q(n)\right|\left|F_q(k)\right| \cos\left(\angle t_q(n) + \angle F_q(k)\right)\right)^2 + \left(\mathrm{Re}\left\{\boldsymbol{\Psi}_{(n)}(k)\right\}\right)^2 + 2\left(\sum_{q=1}^{Q} \left|t_q(n)\right|\left|F_q(k)\right| \cos\left(\angle t_q(n) + \angle F_q(k)\right)\right)\left(\mathrm{Re}\left\{\boldsymbol{\Psi}_{(n)}(k)\right\}\right) + \tag{A-6}$$

$$\left(\sum_{q=1}^{Q}|t_q(n)||F_q(k)|\sin\left(\angle t_q(n)+\angle F_q(k)\right)\right)^2+\left(\mathrm{Im}\left\{\boldsymbol{\Psi}_{(n)}(k)\right\}\right)^2+2\left(\sum_{q=1}^{Q}|t_q(n)||F_q(k)|\sin\left(\angle t_q(n)+\angle F_q(k)\right)\right)\left(\mathrm{Im}\left\{\boldsymbol{\Psi}_{(n)}(k)\right\}\right)$$

By applying a K-point DFT to N_s subsequent snapshots, the average over N_s snapshots approaches the expected value denoted by $E[\ \ ]$ when N_s goes to infinity:

$$\begin{aligned}
&E\left[\left|\boldsymbol{X}_{(n)}(k)\right|^2\right]= \\
&\quad E\left[\left(\sum_{q=1}^{Q}|t_q(n)||F_q(k)|\cos\left(\angle t_q(n)+\angle F_q(k)\right)\right)^2\right]+E\left[\left(\mathrm{Re}\left\{\boldsymbol{\Psi}_{(n)}(k)\right\}\right)^2\right] \\
&+E\left[2\left(\sum_{q=1}^{Q}|t_q(n)||F_q(k)|\cos\left(\angle t_q(n)+\angle F_q(k)\right)\right)\left(\mathrm{Re}\left\{\boldsymbol{\Psi}_{(n)}(k)\right\}\right)\right] \\
&+E\left[\left(\sum_{q=1}^{Q}|t_q(n)||F_q(k)|\sin\left(\angle t_q(n)+\angle F_q(k)\right)\right)^2\right]+E\left[\left(\mathrm{Im}\left\{\boldsymbol{\Psi}_{(n)}(k)\right\}\right)^2\right] \\
&+E\left[2\left(\sum_{q=1}^{Q}|t_q(n)||F_q(k)|\sin\left(\angle t_q(n)+\angle F_q(k)\right)\right)\left(\mathrm{Im}\left\{\boldsymbol{\Psi}_{(n)}(k)\right\}\right)\right]
\end{aligned} \tag{A-7}$$

To simplify equation (A-7), we need to find the expected value of the real and imaginary parts of $\boldsymbol{\Psi}_{(n)}(k)$ and their squares. By using a Cartesian representation, $\boldsymbol{\Psi}_{(n)}(k)$ can be expanded as:

$$\boldsymbol{\Psi}_{(n)}(k)=\sum_{i=0}^{M-1}\eta_i(n)e^{-j\frac{2\pi}{K}ik}=\sum_{i=0}^{M-1}\left(\mathrm{Re}\left\{\eta_i(n)\right\}+j\ \mathrm{Im}\left\{\eta_i(n)\right\}\right)\left(\cos\left(\frac{2\pi}{K}ik\right)-j\sin\left(\frac{2\pi}{K}ik\right)\right) \tag{A-8}$$

According to equation (A-8), the real and imaginary parts of $\boldsymbol{\Psi}^{(n)}(k)$ are given by:

$$\begin{aligned}
\mathrm{Re}\left\{\boldsymbol{\Psi}_{(n)}(k)\right\}&=\sum_{i=0}^{M-1}\left(\mathrm{Re}\left\{\eta_i(n)\right\}\cos\left(\frac{2\pi}{K}ik\right)+\mathrm{Im}\left\{\eta_i(n)\right\}\sin\left(\frac{2\pi}{K}ik\right)\right) \\
\mathrm{Im}\left\{\boldsymbol{\Psi}_{(n)}(k)\right\}&=\sum_{i=0}^{M-1}\left(\mathrm{Im}\left\{\eta_i(n)\right\}\cos\left(\frac{2\pi}{K}ik\right)-\mathrm{Re}\left\{\eta_i(n)\right\}\sin\left(\frac{2\pi}{K}ik\right)\right)
\end{aligned} \tag{A-9}$$

Since the noise is temporally and spatially white Gaussian, we get:

$$E\left[\mathrm{Re}\left\{\boldsymbol{\Psi}_{(n)}(k)\right\}\right] = \sum_{i=0}^{M-1}\left(E\left\{\mathrm{Re}\left\{\eta_i(n)\right\}\right\}\cos\left(\frac{2\pi}{K}ik\right) + E\left\{\mathrm{Im}\left\{\eta_i(n)\right\}\right\}\sin\left(\frac{2\pi}{K}ik\right)\right) = 0$$
$$E\left[\mathrm{Im}\left\{\boldsymbol{\Psi}_{(n)}(k)\right\}\right] = \sum_{i=0}^{M-1}\left(E\left\{\mathrm{Im}\left\{\eta_i(n)\right\}\right\}\cos\left(\frac{2\pi}{K}ik\right) - E\left\{\mathrm{Re}\left\{\eta_i(n)\right\}\right\}\sin\left(\frac{2\pi}{K}ik\right)\right) = 0 \quad \text{(A-10)}$$

Also, according to equation (A-9):

$$\begin{aligned}\left(\mathrm{Re}\left\{\boldsymbol{\Psi}_{(n)}(k)\right\}\right)^2 = &\sum_{i=0}^{M-1}\left(\mathrm{Re}\left\{\eta_i(n)\right\}\right)^2\cos^2\left(\frac{2\pi}{K}ik\right) + \sum_{i=0}^{M-1}\left(\mathrm{Im}\left\{\eta_i(n)\right\}\right)^2\sin^2\left(\frac{2\pi}{K}ik\right)\\ &+2\sum_{i=0}^{M-2}\sum_{p=i+1}^{M-1}\mathrm{Re}\left\{\eta_i(n)\right\}\,\mathrm{Im}\left\{\eta_p(n)\right\}\cos\left(\frac{2\pi}{K}ik\right)\sin\left(\frac{2\pi}{K}pk\right)\\ &+2\sum_{i=0}^{M-2}\sum_{p=i+1}^{M-1}\mathrm{Re}\left\{\eta_i(n)\right\}\,\mathrm{Re}\left\{\eta_p(n)\right\}\cos\left(\frac{2\pi}{K}ik\right)\cos\left(\frac{2\pi}{K}pk\right)\\ &+2\sum_{i=0}^{M-2}\sum_{p=i+1}^{M-1}\mathrm{Im}\left\{\eta_i(n)\right\}\,\mathrm{Im}\left\{\eta_p(n)\right\}\sin\left(\frac{2\pi}{K}ik\right)\sin\left(\frac{2\pi}{K}pk\right)\end{aligned} \quad \text{(A-11)}$$

by applying expected value to both sides of equation (A-11) and considering that the noise is white Gaussian:

$$E\left\{\mathrm{Re}\left\{\boldsymbol{\Psi}_{(n)}(k)\right\}^2\right\} = M\sigma^2 \quad \text{(A-12)}$$

Where $\sigma^2 = E[(Re\{\eta_i(n)\})^2] = E[(Im\{\eta_i(n)\})^2]$

Following the same procedure for the imaginary part in equation (A-9) would result in:

$$E\left\{\mathrm{Im}\left\{\boldsymbol{\Psi}_{(n)}(k)\right\}^2\right\} = M\sigma^2 \quad \text{(A-13)}$$

By considering the independence of background noise from all sources, and substituting equations (A-10), (A-12) and (A-13) into equation (A-7), we get:

$$E\left[\left|\boldsymbol{X}_{(n)}(k)\right|^2\right] = E\left\{\left(\sum_{q=1}^{Q}\left|t_q(n)\right|\left|F_q(k)\right|\cos\left(\angle t_q(n)+\angle F_q(k)\right)\right)^2 + \left(\sum_{q=1}^{Q}\left|t_q(n)\right|\left|F_q(k)\right|\mathrm{Sin}\left(\angle t_q(n)+\angle F_q(k)\right)\right)^2\right\} + 2M\sigma^2 \quad \text{(A-14)}$$

Each term inside the bracket in equation (A-14) can be expressed as:

$$\left(\sum_{q=1}^{Q}\left|t_q(n)\right|\left|F_q(k)\right|\cos\left(\angle t_q(n)+\angle F_q(k)\right)\right)^2 = \sum_{q=1}^{Q}\left|t_q(n)\right|^2\left|F_q(k)\right|^2\cos^2\left(\angle t_q(n)+\angle F_q(k)\right) + 2\sum_{q=1}^{Q-1}\sum_{p=q+1}^{Q}\left|t_q(n)\right|\left|t_p(n)\right|\left|F_q(k)\right|\left|F_p(k)\right|\cos\left(\angle t_q(n)+\angle F_q(k)\right)\cos\left(\angle t_p(n)+\angle F_p(k)\right) \quad \text{(A-15)}$$

And

$$\left(\sum_{q=1}^{Q}\left|t_q(n)\right|\left|F_q(k)\right|\sin\left(\angle t_q(n)+\angle F_q(k)\right)\right)^2 = \sum_{q=1}^{Q}\left|t_q(n)\right|^2\left|F_q(k)\right|^2\sin^2\left(\angle t_q(n)+\angle F_q(k)\right) + 2\sum_{q=1}^{Q-1}\sum_{p=q+1}^{Q}\left|t_q(n)\right|\left|t_p(n)\right|\left|F_q(k)\right|\left|F_p(k)\right|\sin\left(\angle t_q(n)+\angle F_q(k)\right)\sin\left(\angle t_p(n)+\angle F_p(k)\right) \quad \text{(A-16)}$$

substituting equations (A-15) and (A-16) into equation (A-14) we get:

$$E\left[\left|\boldsymbol{X}_{(n)}(k)\right|^2\right] = E\left[\left|t_q(n)\right|^2\left|F_q(k)\right|^2 + 2\sum_{q=1}^{Q-1}\sum_{p=q+1}^{Q}\left|t_q(n)\right|\left|t_p(n)\right|\left|F_q(k)\right|\left|F_p(k)\right|\cos\left(\angle t_q(n)-\angle t_p(n)+\angle F_q(k)-\angle F_p(k)\right)\right] + 2M\sigma^2 \quad \text{A-17)}$$

Since $t_q(n)$ is a zero-mean random variable, accordingly, $t_q(n) - t_p(n)$ is a zero-mean random variable. This implies that $t_q(n) - t_p(n)$ is statistically symmetric around the origin, i.e. in a statistical sense the probability of generating $|A|e^{j(\angle\varphi)}$ is equal to that for $|A|e^{j(\angle\varphi+\pi)}$. Consequently, it can be shown that the expected value of $cos\big(\angle t_q(n) - \angle t_p(n) + \angle F_q(k) - \angle F_p(k)\big)$ is zero. Note that $\angle F_q(k) - \angle F_p(k)$ can be treated as a constant over the time index and the expected value of an arbitrary function (g) of a random discrete variable $\boldsymbol{X}$ is:

$$E[g(\boldsymbol{X})] = \sum_x g(x)f(x) \tag{A-18}$$

Where f is the probability distribution function and the sigma is over all possible cases for $\boldsymbol{X}$. thus**:**

$$E\big[cos\big(\angle t_q(n) - \angle t_p(n) + \angle F_q(k) - \angle F_p(k)\big)\big] = \sum_i cos\big(\Delta_i + \angle F_q(k) - \angle F_p(k)\big)\, f(\Delta_i) \tag{A-19}$$

Where $\Delta_i = \angle t_q(n) - \angle t_p(n)$ is randomly scattered around the origin of the complex plane with a uniform distribution. Therefore, if the probability of Δ_i equal to $\emptyset_i$ is ρ, $\emptyset_i + \pi$ would occur with the same probability.

$$\begin{aligned} &E\left[cos\left(\angle t_q(n) - \angle t_p(n) + \angle F_q(k) - \angle F_p(k)\right)\right] = \\ &\sum \rho\cos\big(\emptyset_i + \angle F_q(k) - \angle F_p(k)\big) + \rho\cos\big(\emptyset_i + \pi + \angle F_q(k) - \angle F_p(k)\big) = 0 \end{aligned} \tag{A-20}$$

Further, by calculating the covariance between $\big|t_q(n)\big|\big|t_p(n)\big|$ and $cos\big(\angle t_q(n) - \angle t_p(n) + \angle F_q(k) - \angle F_p(k)\big)$, it can be proved that they are uncorrelated (not necessarily independent), i.e., their covariance is equal to zero. Therefore, the expected value of their product can be replaced by the product of their expected values. Also, since all *Q* sources are independent, $\big|t_q(n)\big|$ and $\big|t_p(n)\big|$

are independent and accordingly uncorrelated resulting in $E\left[\left|t_q(n)\right|\left|t_p(n)\right|\right] = E\left[\left|t_q(n)\right|\right]E\left[\left|t_p(n)\right|\right]$ By substituting:

$$\begin{aligned} \mathfrak{k}_q &= E\left|t_q(n)\right| \qquad\qquad for\ 1 \le q \le Q \\ \zeta_q &= E\left|t_q(n)\right|^2 \end{aligned} \tag{A-21}$$

into equation (A-17), it can be concluded that:

$$E\left\{\left|\boldsymbol{X}_{(n)}(k)\right|^2\right\} = \Gamma_1(k) + \Gamma_2(k) + 2M\sigma^2 \tag{A-22}$$

Where:

$$\Gamma_1(k) = \sum_{q=1}^{Q} \zeta_q \left|F_q(k)\right|^2 \tag{A-23}$$

$$\Gamma_2(k) = 2\sum_{q=1}^{Q-1}\sum_{p=q+1}^{Q} \mathfrak{k}_q\mathfrak{k}_p\left|F_q(k)\right|\left|F_p(k)\right| \mathrm{E}\left[\cos\left(\angle t_q(n) - \angle t_p(n) + \angle F_q(k) - \angle F_p(k)\right)\right] \tag{A-24}$$

As was discussed, $E\left[\cos\left(\angle t_q(n) - \angle t_p(n) + \angle F_q(k) - \angle F_p(k)\right)\right]$ is equal to zero resulting in:

$$\Gamma_2(k) = 0 \tag{A-25}$$

Therefore, equation (A-22) can be simplified as:

$$E\left\{\left|\boldsymbol{X}_{(n)}(k)\right|^2\right\} = \Gamma_1(k) + 2M\sigma^2 \qquad for \qquad -l \le k \le l \tag{A-26}$$

By replacing $F_q(k)$ from equation (A-2) in equation (A-23), we get:

$$\Gamma_1(k) = \sum_{q=1}^{Q} \zeta_q \left(\frac{\sin\left(\frac{\pi d\,\cos(\theta_q)}{\lambda} + \frac{\pi k}{K}\right) M}{\sin\left(\frac{\pi d\,\cos(\theta_q)}{\lambda} + \frac{\pi k}{K}\right)}\right)^2 \tag{A-27}$$

■